

Neurocase

The Neural Basis of Cognition

ISSN: 1355-4794 (Print) 1465-3656 (Online) Journal homepage: <http://www.tandfonline.com/loi/nncs20>

Applying fMRI complexity analyses to the single subject: a case study for proposed neurodiagnostics

Anca R. Rădulescu & Emily R. Hannon

To cite this article: Anca R. Rădulescu & Emily R. Hannon (2017) Applying fMRI complexity analyses to the single subject: a case study for proposed neurodiagnostics, *Neurocase*, 23:2, 120-137, DOI: [10.1080/13554794.2017.1316410](https://doi.org/10.1080/13554794.2017.1316410)

To link to this article: <http://dx.doi.org/10.1080/13554794.2017.1316410>



Published online: 31 May 2017.



Submit your article to this journal [↗](#)



Article views: 18



View related articles [↗](#)



View Crossmark data [↗](#)

Full Terms & Conditions of access and use can be found at
<http://www.tandfonline.com/action/journalInformation?journalCode=nncs20>



Applying fMRI complexity analyses to the single subject: a case study for proposed neurodiagnostics

Anca R. Rădulescu^a and Emily R. Hannon^b

^aDepartment of Mathematics, SUNY, New Paltz, NY, USA; ^bDepartment of Ecology and Evolutionary Biology, University of Colorado at Boulder, Boulder, CO, USA

ABSTRACT

Nonlinear dynamic tools have been statistically validated at the group level to identify subtle differences in system wide regulation of brain meso-circuits, often increasing clinical sensitivity over conventional analyses alone. We explored the feasibility of extracting information at the single-subject level, illustrating two pairs of healthy individuals with psychological differences in stress reactivity. We applied statistical and nonlinear dynamic tools to capture key characteristics of the prefrontal-limbic loop. We compared single subject results with statistical results for the larger group. We concluded that complexity analyses may identify important differences at the single-subject level, supporting their potential towards neurodiagnostic applications.

ARTICLE HISTORY

Received 8 December 2015
Accepted 30 March 2017

KEYWORDS

Stress reactivity; fMRI; single-subject analysis; principal components; power spectrum scale invariance

1. Introduction

Historically, neuroimaging has focused on measuring the amplitude of activation levels in different regions of interest for some specific task, or for resting state. In the past few years, newer connectivity methods such as structural equation modeling (Büchel & Friston, 1997; Kim, Zhu, Chang, Bentler, & Ernst, 2007), Granger causality (Roebroeck, Formisano, & Goebel, 2005), and dynamic causal modeling (Friston, Harrison, & Penny, 2003) have increased in popularity. Designed to address effective connectivity, defined as the directional influence that one neural region exerts over another, these methods investigate temporal components of the time series. A different approach builds upon this work to ask how a negative feedback loop as a whole responds to perturbation in the maintenance of homeostasis. This represents a marked departure from investigating node-specific amplitude fluctuations, or their correlation between node pairs, and instead uses tools from nonlinear dynamics. These tools have been used primarily in conjunction with statistics, for subject classification into behavioral groups or for differentiation between patient and control populations.

It has been argued that since the vast majority of fMRI studies present group averaged data, it is possible that the typical imaging findings may capture only one of many potential neural mechanisms subserving the same cognitive function (Friston & Price, 2003). Moreover, fMRI statistics are liable to produce misleading results, not only through inappropriate use of statistical measures (e.g., uncorrected or overcorrected data) but also due to intrinsic limitations of statistical tools. Following up Huff's (1954) classic book *How to Lie with Statistics*, Culham (2006) synthesizes some of the drawbacks of using statistical methods in neuroimaging to readily draw conclusions about subject groups. For example,

group averaged data (as in Talairach space) are the standard way to extract the group's general pattern and notice trends that may not be obvious in single subjects. However, interpreting group average data by itself can be misleading. For example, if there is high anatomical variability in the focus of activation, there may not be enough overlap for an area to show up in the group averaged data. Moreover, in order to perform statistical comparisons, neural data from all subjects are transformed (e.g., resliced and normalized), making temporal and spatial assumptions that are not necessarily valid for all individuals, and thus introducing confounds in the results.

On the other hand, case studies, while more suitable to pin down which mechanisms are necessary for a given function, encounter a range of distinct problems, primarily related to signal-to-noise ratio, to the high variability between individuals, and to the equally high heterogeneity of behavioral symptoms. In "Neuroimaging of single cases: benefits and pitfalls" (Danckert, Mirsattari, & Bright, 2012), the authors discuss the small proportion of case studies versus group statistical studies in the current neuroimaging literature, they point out benefits and shortcomings, and propose a combination of the two approaches as the best way to advance our understanding of brain regulation and function (see also Chatterjee, 2005; Friston & Price, 2003).

In this paper, we aim to illustrate how case study analyses could complement existing statistically based results, providing more focused information to help build a schematic brain profile of each subject at hand. In conjunction with statistical analyses of a larger group of subjects, we considered two particular subject pairs so that the two subjects in each pair had very different emotional profiles: one normally responsive to stress, and the other

exceptionally nonreactive to stress. We applied a combination of linear and nonlinear analyses of amplitude, correlation and signal frequency spectra, emphasizing for each subject the interplay within a network of brain areas – either known a priori to contribute to emotion regulation or discovered to be involved through whole brain exploratory analyses. Instead of statistical tests, we used a system of comparisons and thresholding, with the threshold values established through a fine-tuning process, designed to identify the most prominent patterns. We then computed differences between the two cases and performed a customized analysis for each subject, as well as comparisons between all.

1.1. Complexity measures for fMRI

Complexity analyses of physiological data have gained popularity in cardiology because their results provide clinically valuable diagnostic information (Huikuri et al., 2000; Montano et al., 1994; Stamkopoulos, Diamantaras, Maglaveras, & Strintzis, 1998). More recently, complexity has been documented in the brain, at many levels of neural function (He, 2014; Ide, Sien, Zhang, Mujica-Parodi, & Li Chiang-Shan, 2016), from neurotransmitter release (Lowen, Cash, Poo, & Teich, 1997), spiking activity (Levina, Michael Herrmann, & Geisel, 2007; Rubinov, Sporns, Thivierge, & Breakspear, 2011), local field potentials (Bédard & Destexhe, 2009), slow cortical potentials (He & Raichle, 2009), and electroencephalography (Freyer, Aquino, Robinson, Ritter, & Breakspear, 2009).

There is now evidence that dynamic invariants can be used diagnostically in identifying pathology in conjunction with a variety of modalities: EEG (Daneshyari, Lily Kamkar, & Daneshyari, 2010), MEG (Stam, 2005), NIRS (Xiao-Su, Hong, & Ge, 2011), and fMRI. This suggests the importance in examining the complexity neural signals across multiple scales. Recent research suggests complexity measures of BOLD signals as an important neural marker in the healthy brain (Anderson, Zielinski, Nielsen, & Ferguson, 2014; Bassett & Gazzaniga, 2011; Ciuciu, Abry, & He, 2014; He, Zempel, Snyder, & Raichle, 2010) as well as in neuropsychiatric conditions (He et al., 2010; Lai et al., 2010; Maxim et al., 2005; Rădulescu, Rubin, Strey, & Mujica-Parodi, 2012; Tolkunov, Rubin, & Lilianne R, 2010).

Complexity measures have been used to identify both between-voxel and between-subject differences. For example, active and inactive voxels in the human visual cortex showed different complexity (measured as power-law and Hurst exponents) during a visual task (Thurner, Windischberger, Moser, & Barth, 2002). More recent results found different voxel-wise values of the power law exponent (Bandettini et al., 2008; Bullmore et al., 2009) across different functional networks (e.g., attention, default, motor, saliency, and visual) (He et al., 2010), across cognitive loads (Barnes, Bullmore, & Suckling, 2009; Suckling, Wink, Bernard, Barnes, & Bullmore, 2008), as well as more generally between active and non-active voxels (Shimizu, Barth, Windischberger, Moser, & Thurner, 2004).

Theoretically, complexity and scale invariance measures in brain physiology are to be optimally applied to time

series that are long, rich, and have strong signal-to-noise ratio, similarly with 24-h ECG. In contrast, fMRI time series tend to be short (5–10 min), sparse (up to TR = 2.5 s), and subject to sufficient scanner and physiological artifacts that significant preprocessing is most often required. As discussed above, there is increasing evidence supporting sensitivity of complexity measures in differentiating between mental conditions using fMRI. However, temporal analyses of fMRI time courses require careful modality-specific optimization, and careful consideration of whether the techniques have sufficient signal-to-noise ratio to provide information, in particular in the context of single-subject analyses.

A few papers in the recent literature suggest different methods for being best-suited to describe scale invariance and chaotic behavior in fMRI data. Some studies have found that, under certain circumstances, fMRI time series are well approximated by stationary processes with a linear log–log spectrum so that their scale invariance can be captured by simply estimating the slope of the log–log spectrum. Other studies have suggested that fMRI signals are best modeled by multifractal processes (Ciuciu, Varoquaux, Abry, Sadaghiani, & Kleinschmidt, 2012; Wink, Bullmore, Barnes, Bernard, & Suckling, 2008).

A lot of effort has been invested in optimizing scale invariance computations in fMRI time series. In order to reconcile the most popular of these methods, Rubin, Fekete, and Mujica-Parodi (2013) performed a systematic comparative analysis of complexity computation methods, specifically for fMRI signals. In their work, the authors discuss the challenges associated with each method, investigate the effects of data preprocessing, activation, and scanner differences, with a focus on optimizing the balance between detection sensitivity and resilience to artifacts. The methods investigated in the reference are power spectrum, structure function, wavelet decomposition, second derivative, rescaled range, Higuchi's estimate of fractal dimension, aggregated variance, and detrended fluctuation analysis. To permit direct comparison across methods, all results were normalized to Hurst exponents. The authors showed that complexity measures are highly correlated but have different sensitivity and susceptibility to fMRI-specific artifacts and other external factors. These factors (choice of algorithm, signal processing, time-series length, and scanner) interact with complexity calculations in nontrivially distinct ways and ultimately have a significant impact on the reliability and sensitivity of complexity estimates.

The reference above bares more than theoretical relevance onto our current study. That is because the fMRI data in the current case study are identically aligned with one of the datasets analyzed in the reference (in task design, acquisitions parameters, and even physical scanner). Hence, when selecting the optimal complexity measures to use for our current analysis, we naturally followed the conclusions in the reference, in which power spectrum, Higuchi's fractal dimension, and generalized Hurst exponent estimates were most successful by all criteria employed (while other complexity measures such as wavelet based estimates, detrended fluctuation analysis, aggregated variance, and

rescaled range were found to have a poor performance). Based on this, we chose to investigate in our single subjects a set of three different measures of complexity: power-spectral scale invariance, generalized Hurst exponent, and approximate entropy (ApEn).

1.1.1. Power spectrum scale invariance

The dynamic patterns in a network's stationary oscillations can be captured in the frequency domain by Fourier analysis, using the power-spectral density of the signals recorded from the network's nodes. A classical measure used to estimate the complexity of the signals consists of expressing the mean square fluctuations at any particular frequency f , and how these vary with frequency. Power spectrum scale invariance (PSSI) means that there is no preferred temporal scale and that the power-spectrum density of the signal follows a power-law behavior: $S(f) \sim f^\beta$ (He et al., 2010). In this context, the scaling exponent β is close to 0 (white noise) at maximum entropy/chaos, and $\beta < 0$ represents increasing regularity.

Scale-free properties of brain activity as captured from fMRI signals have been the subject of intense investigation over the past decade (Bullmore et al., 2001). Originally thought of as structured (or fractal) noise, scale-free brain activity in brain networks has been shown in newer studies to be rather a product of rich coupled dynamics in the network, and PSSI values are believed to hold functional significance (Boustani et al., 2009; Ciuciu et al., 2014; Fransson et al., 2013; He, 2011; He et al., 2010). Indeed, empirical PSSI values were correlated with signal variance across different brain regions (He, 2011), with larger values for default-mode, saliency, and visual networks (Fransson et al., 2013; He, 2011). In addition, recent studies reported altered fMRI signal complexity in task-induced activations (Bianciardi et al., 2009; Fransson, 2006; He, 2011) as compared to resting state, supporting the idea that brain activity reflects even in the second-order statistics of fMRI signals, and ruling out the possibility that scale-free property of brain activity is simply noise.

In terms of neural excitability, results can be interpreted as brain efficiency, increasing when β is decreased (i.e., the lower β , the more reactive the brain). Statistical studies that have applied PSSI analyses to clinical fMRI have shown, for example, that β is higher at rest as compared to task because when you're engaged in task performance, the serial correlation in the time series becomes shorter (Ciuciu et al., 2014, 2012; He, 2011). Healthy neurobiological states are characterized by roughly $\beta = -1$ (signals with spectra $S(f) = f^{-1}$ are known as pink, or $1/f$ noise), while pathological neural time series may be significantly shifted in either direction. Our prior work demonstrated that as a neural circuit becomes increasingly dysregulated in a neurological or neuropsychiatric illness, signal complexity of the affected nodes deviates from an equilibrium value – as observed in trait anxiety, epilepsy, and schizophrenia (Mujica-Parodi, Carlson, Cha, & Rubin, 2014; Nedic et al., 2015; Rădulescu et al., 2012; Tolkunov et al., 2010).

New evidence also suggests that connectivity may play a key role in establishing the complexity of BOLD signals (Anderson et al., 2014). Ourselves and others have investigated mathematically the possibility that PSSI may be attained in the brain as a form of meta-stability of a network in which a large number of neural oscillators couple and decouple in response to stimuli and network feedback (Buzsaki, 2006; Rădulescu, 2014).

1.1.2. The Hurst exponent

The Hurst exponent is also a measure of long-term memory of time series, describing the rate at which autocorrelation decreases as the lag increases. Even for a nonstationary process $X(t)$, which is often the case in brain signals, one may still end up with self-similar stationary increments whose statistical moments of all orders $q > 0$ have power-law behavior characterized by a single-scaling exponent $H = H(q)$ (the Hurst exponent): $\langle |X(t + \tau) - X(t)|^q \rangle = c_q |\tau|^{qH}$, where τ is the time lag, and the average $\langle \cdot \rangle$ is over the time window. The values of the Hurst exponent vary between 0 and 1, with higher values indicating a smoother trend, less volatility, and less roughness. A value of H in the range 0.5–1 indicates a time series with long-term positive autocorrelation; a value in the range 0–0.5 indicates a time series with long-term switching between high and low values in adjacent pairs. There are a variety of techniques that exist for estimating H from physiological time series (He, 2011; Maxim et al., 2005), with accuracy depending on the data properties (Rubin et al., 2013). For example, in fMRI data, H was found to be increased in the early regions involved in the neurodegenerative process of Alzheimer's disease (Maxim et al., 2005). For structured noise, the Hurst parameter can be computed from the PSSI value β through the relationship $H = (|\beta| - 1)/2$ (Schaefer, Brach, Perera, & Ervin, 2014). For example, $H = 0.5$ for Brown noise (when $\beta = -2$), and $H = 0$ for pink noise (when $\beta = -1$). When $H(q)$ is a nonlinear function of q , the underlying process $X(t)$ (associated with the measured fMRI time series) is multifractal (Ciuciu et al., 2012; Wink et al., 2008).

1.1.3. Approximate entropy

ApEn was introduced in 1991 (Pincus, 1991) as an entropy measure that can be applied computationally to biological systems, with a successful handle on the noise and shortness of biological data streams (Pincus, 2003; Pincus & Singer, 1996). A variety of early studies used ApEn to quantify heart rate (Ryan, Goldberger, Pincus, Mietus, & Lipsitz, 1994) and respiration variability (Engoren, 1998), endocrine activity in dysregulatory conditions (Roelfsema, Pincus, & Veldhuis, 1998; Schmitz et al., 1997), to predict epileptic seizures from EEG data (Radhakrishnan & Gangadhar, 1998), and to analyze bipolar (Glenn et al., 2006; Pincus, 2006), depressive, and schizophrenic courses (Paulus, Geyer, & Braff, 1996; Pezard et al., 1996; Tschacher, Scheier, & Hashimoto, 1997) from behavioral data. ApEn has reemerged in newer studies as a physiologically and functionally meaningful measure for studying brain functions (Wang, Yin, Childress, & Detre,

2014), and in particular as a potentially sensitive method for the complexity analysis of fMRI time courses (Sokunbi, Cameron, Ahearn, Murray, and Staff, 2015).

In our case study, we used all three complexity methods. For the purposes of this paper, we chose to illustrate here the results obtained with PSSI, which were strongest, and additionally describe results for ApEn in Appendix A. This also allows us to compare the single-subject results with our prior statistical results (described below), and to reconcile the conclusions with our theoretical modeling work, in which we have also used the same PSSI to measure complexity of our simulated solutions. As a proof of principle, we illustrate that the method that we have used in our previous work in conjunction with statistics on identical or similar datasets can be applied as single-subject analyses to obtain individually customized results (brain-profiling), which confirm or can even explain the statistics.

1.2. PSSI and prior results

Prior work leading to this study involved two fMRI datasets [S1, previously described in Tolkunov et al. (2010), and S2, previously described in Carlson, Greenberg, Rubin, and Mujica-Parodi (2011)]. These two sets included overall 96 individuals, ranging emotionally from extremely reactive to extremely nonreactive. The average-to-reactive range ($n = 65$) was identified using clinical questionnaires (study S1), while the average-to-nonreactive range ($n = 31$) was identified using cortisol response in anticipation of a first-time skydive (study S2). These two datasets were used in our previous work (Carlson et al., 2011; Tolkunov et al., 2010) to study the circuit response efficiency, using power-spectral scale invariance (PSSI) of brain signals.

For all PSSI analyses (for both S1 and S2), we used minimally preprocessed fMRI BOLD time series, which included all conditions. Using methods previously optimized for fMRI (Rubin et al., 2013), we calculated for each voxel the power-spectral density as the squares of the Fourier transformation amplitudes of the linearly detrended time series. We first verified that our power spectra indeed obey a power law, by fitting several common candidate distributions to sample spectra of our longest time series. From the power-spectral density, we computed the scaling parameter β by plotting the power spectrum on a log-log scale and estimating the slope by applying a linear fit to the data in a frequency range chosen to avoid confounds due to either task design or physiological variables such as heart rate or respiration.

Individuals who were in the middle range of the spectrum had β values in the pink noise range, for both the amygdala (excitatory) and prefrontal (inhibitory) areas. Individuals who were more fearful showed limbic β values closer to 0, localized to the amygdala. Individuals who were more fearless also showed limbic β values closer to 0 but localized to the prefrontal cortex. These results fall within the general interpretation of complexity in terms of brain efficiency: $\beta \sim 0$ in the amygdala represents an efficient excitatory drive, which explains the higher sensitivity to fear stimuli in this subject group; $\beta \sim 0$ in prefrontal areas represents increased efficiency in inhibitory regulation and may explain the increased resilience to fear stimuli.

In our modeling work (Rădulescu, 2014), we suggested a testable framework for interpreting and unifying these results in terms of prefrontal-limbic regulation, and emotional control efficiency. In this study, we aim to verify if these results hold qualitatively at a single-subject level, and whether single-subject analyses *within* the subject groups may provide more complete explanations or may reveal additional trends which escaped the general statistics.

2 Methods

2.1. Subjects

2.1.1. Dataset

In order to provide a consistent and informative comparison of single-subject versus statistical approaches, we focused on the dataset obtained through S2. This study was approved by the institutional review board at Stony Brook University; all subjects provided written informed consent. Twenty-three healthy adults between the ages of 18 and 48 participated in one of the two versions of the study (the differences between the two versions being of imaging task design). A lengthy phone screening, as well as the scheduled clinical interview for DSM-IV, was administered to rule out subjects with current or prior psychiatric illness. All subjects received a history questionnaire and a physical exam; subjects were excluded if they had a history of drug abuse, traumatic brain injury, cardiovascular illness (including high blood pressure), regular nicotine use, or any MRI exclusion criteria, including metal in the body, claustrophobia, or pregnancy/lactation. Trait anxiety scores ranged from 20 to 53.

2.1.2. Case studies

As the first of our case study pairs, we chose specifically two subjects in S2 which were tested as part of an original study for the Discovery Channel for their popular science television series *Curiosity*. The show aimed to illustrate how functional neuroimaging might one day be used for neurodiagnostics, by taking two subjects with known differences in stress reactivity (based upon their professions), and then determining if fMRI was able to identify differences. One of the subjects, D, was a biology Ph.D. (average stress reactivity); the other, T, was an explosive ordinance disposal technician working in support of US Navy SEAL missions [with exceptional nonreactivity to stress and sensation-seeking behavior (Mujica-Parodi et al., 2014)]. The second case study pair was chosen randomly from S2 so that one of the two subjects (subject X) belonged to the high reactivity range, and the other one (subject Y) to the low reactivity range.

2.2. Imaging design

The fMRI task, a block design using countdowns to imminent aversive or benign noise, has previously been described (Carlson et al., 2011) and is summarized briefly in Section 2.4. Subjects were scanned on a 3-T Siemens Trio MRI scanner at the Stony Brook University SCAN Center using a 12-channel SENSE parallel head coil. Data were acquired using 232 T2*-weighted echo planar single-shot images covering the whole brain (oblique coronal) with the following parameters: TR = 2500 ms, SENSE factor = 2,

TE = 22 ms, flip angle = 83° , matrix dimensions = 96×96 , FOV = 224×224 mm, slices = 36, slice thickness = 3.5 mm, gap = 0. The anatomical data were used to generate a customized echo planar imaging (EPI) template to normalize our EPI scans to the standard frame of reference. The fMRI data analyses were performed using the Statistical Parametric Mapping software (SPM8; <http://www.fil.ion.ucl.ac.uk/spm>), using MATLAB 2010a. Standard preprocessing procedures were performed, including image realignment corrections for head movements, slice timing corrections for acquisition order, normalization-to-standard $2 \times 2 \times 2$ mm Montreal Neurological Institute space, and spatial smoothing with a 6-mm full width at half maximum Gaussian kernel.

2.3. Stimuli and equipment

The auditory anticipation task included both auditory events and visual cues. All visual stimuli were presented using a mirror attached to the head coil, which reflected onto a screen positioned behind participants while they lay in the scanner. Visual stimuli were presented on the screen using an MRI-compatible 60-Hz projector with a 1024×768 resolution. Auditory stimuli were presented through SereneSound (Resonance Technology Inc., Northridge, CA, USA) 30-dB external noise attenuating MRI-compatible headphones. Auditory and visual stimuli were presented and the task was programmed with E-Prime 1.2 (Psychology Software Tools, Pittsburg, PA, USA). Initiation of the experiment was triggered by the first radiofrequency pulse of the EPI sequence.

2.4. Experimental procedure

The auditory anticipation task consisted of 20 trials/blocks of anticipation: 10 aversive and 10 neutral. Each trial began with

a white fixation cue presented in the center of a black screen (jittered 4000–8000 ms). The fixation cue was immediately followed by a red X or a blue O for 1000 ms. Participants were informed that the red X indicated that they would hear a loud 100-dB burst of white noise (aversive event), while the blue O indicated that they would hear a soft (55-dB) presentation of the same white noise (neutral event). Preceding the presentation of aversive and neutral events was a 16-s period (block) of anticipation. During this block of anticipation, a countdown from 16 to 1 (16 s; red text for aversive and blue for neutral) was numerically presented in the center of the screen. Aversive and neutral auditory events immediately followed this period of anticipation and were 1000 ms in duration. After the presentation of the aversive or neutral event, a screen appeared which asked participants to rate their level of anxiety during the countdown on a 4-point scale (from 1 = “not anxious” to 4 = “very anxious”).

2.5. Modeling methods

For the first part of the study, we focused on the subject pair from the Discovery dataset (subjects which we will call D and T). This particular pair of individuals was chosen for our study because they were recruited and tested precisely for the purpose of carrying out a single-subject analysis. While they underwent the same series of tests as the larger group S2, these two subjects were specifically chosen in order to illustrate (for a popular science television show) the effectiveness of using imaging methods to distinguish between two individuals with markedly different levels of resilience to stress. We performed a single-subject analysis as well as a comparison between the two, using a variety of methods and measures, as described below.

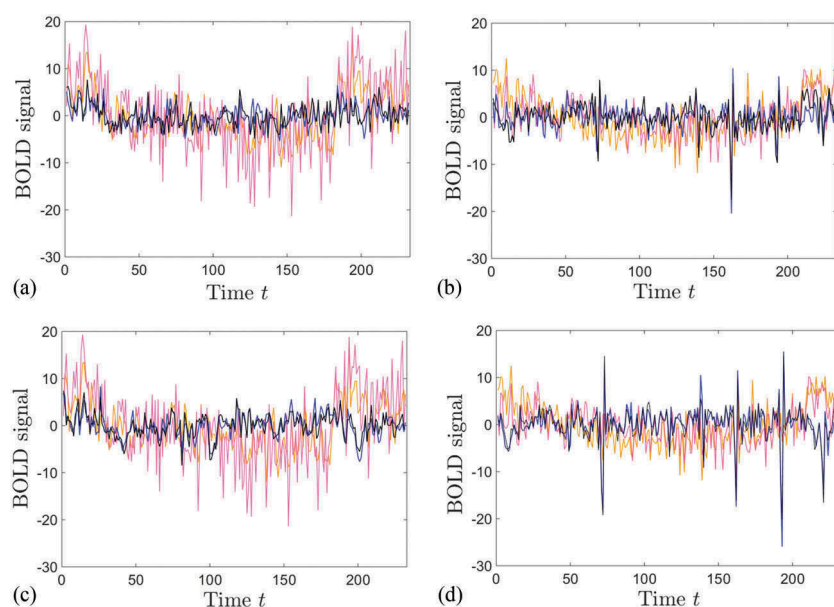


Figure 1. Average time series, for subject D (left) and for subject T (right). We illustrate the whole (232 data points, all conditions included), average detrended time series for the left and right amygdala (light colored curves – orange and pink, respectively) compared to those for the left and right Brodmann Area 45 (top panels, dark color curves – blue and black, respectively) and of the left and right Brodmann Area 9 (bottom panels, blue and black). [To view this figure in color, please see the online version of this journal.]

2.5.1. General linear model

We performed a traditional single-subject activation analysis, as per the general linear model (GLM) provided by the Statistical Parametric Mapping software, with familywise error (FWE) corrected $p < 0.01$, and contiguous volume threshold $V = 64$ voxels (equivalent with the volume of a cube of side 4 voxels). For both subjects, we analyzed the contrasts Anxious > Rest, Rest > Anxious, Neutral > Rest, and Rest > Neutral.

2.5.2. Hypothesis-driven, region of interest analysis

We (Rădulescu, 2014; Rădulescu & Mujica-Parodi, 2008) and others (Banks, Eddy, Angstadt, Nathan, & Phan, 2007; Sotres-Bayon, Bush, & LeDoux, 2004) have shown that the amygdala and prefrontal regions form a negative feedback loop that regulates emotional arousal. Taking this as a starting point for our case studies, we investigated interactions between the amygdala and Brodmann Areas 9 and 45, which we have found in our prior work to reflect efficiency of the individual's emotional responses to stressors (Mujica-Parodi et al., 2009; Rădulescu & Mujica-Parodi, 2008). In fact, gross inspection of the region of interest (ROI) average time series for our case studies in these regions (Figure 1) suggested markedly different temporal evolutions between the two subjects, with a dominant amygdala in subject D, and a dominant prefrontal response in subject T. We investigated this further using a cross-correlation analysis for six bilateral regions of interest: amygdala, inferior frontal gyrus (Brodmann Area 45), dorsolateral prefrontal cortex (Brodmann Area 9), hippocampus, anterior cingulate, and insula. We chose this subnetwork of regions based on their known involvement in emotional regulation (Etkin, Egner, & Kalisch, 2011; Goldin, McRae, Ramel, & Gross, 2008; Ochsner et al., 2004; Phelps, 2004; Phelps & LeDoux, 2005), as well as on our prior group analyses (Mujica-Parodi et al., 2014), suggesting these regions as relevant to emotional processing of stressful stimuli.

One way to approach this 12-dimensional network more comprehensively than by studying its combinations of node pairs is to check if it naturally favors a low-dimensional principal component (PC) subspace. The location and contribution of these PCs can provide better information and additional understanding of the temporal evolution of the system as a whole. To this end, we used a PC analysis to search for the regions within our model network that had the highest contribution to the network dynamics for each individual.

2.5.3. Exploratory analyses

Stepping away from any a priori assumptions, we performed exploratory searches for locations with specific dynamic properties related to amplitude, frequency band and signal regularity, properties that typically suggest involvement of the corresponding brain areas in emotional processing. As per our previous work (Rădulescu et al., 2012; Tolkunov et al., 2010) we calculated, for both subjects, the discrete power spectrum of each voxel-wise time series, using the discrete fast Fourier transform (fft). We performed a best

linear fit to the log-log spectra. We found the spectrum (calculated with both fft and Welch methods) to have close to linear behavior within a band width of 0.025–0.2 Hz (the upper limit is the highest frequency permitted by our temporal sampling resolution, and the lower limit was chosen to insure the goodness of the linear fit). We computed the value of the PSSI slope β corresponding to the respective voxel. Since the results were comparable between the two methods of estimating PSSI (see Appendix B), we work henceforth with the β brain maps obtained with the fft method.

We then used thresholding to search for (1) active voxel clusters within the brain in which β was unusually high or unusually low (compared to the optimal value $\beta = -1$) for either one of the two subjects and (2) regions in which the β values differed substantially between the two subjects. This combination allowed both a direct comparison, and an implicit comparison of the results obtained independently for each of the two subjects. Once these voxel clusters were established, we further analyzed their overall dynamics by calculating the cluster-wise mean PSSI and illustrating the corresponding Pointcaré maps. In order to test the hypothesis that these clusters are in fact part of a *functional network* activated during the fMRI task, we computed to what degree these clusters' activity was more strongly cross-correlated among themselves than with other parts of the brain.

For the second part of the study, we used PSSI to perform a statistical analysis on S2. Our aim was to illustrate how using methods that quantify brain dynamics at the single-subject level can complement the more traditional statistical tests. This may happen (1) by supporting and refining the broader statistical results and (2) by finding additional patterns overlooked by the statistics, hence revealing a bigger picture and clearer connections, and providing a more complete description of the individual's stress-resilience profile. In order to statistically compare low and high-reactivity individuals, we isolated two subgroups within S2, based on their trait anxiety scores: the low-anxiety group ($N = 10$, $TA \in [20, 30]$) and the high-anxiety group ($N = 10$, $TA \in [35, 53]$). We chose to discard the subjects with intermediate scores ($TA \in [31, 34]$), so as to obtain a clearer separation between the two emotional subtypes, without compromising statistical power. For each of these subjects, we calculated the voxel-wise PSSI values. We then performed a Wilcoxon rank sum statistical test on the β values between the two groups, retaining only the voxel clusters with significant p value and with volume above a specific threshold.

Our final goal is to use these results as a proof of principle for the effectiveness of single-subject analyses. However, a generalization of our results may be difficult to claim at this stage, especially since our first subject pair was carefully picked a priori for the study, based on their behavioral traits, so as to maximize the potential for between-subject differences in brain dynamics. In the third part of the study, we took the first steps toward validating the methods in a more general setting, by retesting these methods on an additional subject pair. In contrast with the first pair (D, T), the second pair (X, Y) is randomly

chosen from the low and high-reactivity subgroups of S2. For this new pair, we verify the consistency of our initial conclusions.

3. Results

3.1. First subject pair

3.1.1. GLM

The activation clusters found by the GLM analysis are shown for both subjects in Table 1. In both cases, the Task > Rest contrasts revealed primary visual (occipital) activation regions,

Table 1. Contiguous activation clusters identified by the single-subject GLM analysis (FWE corrected $p < 0.01$, volume $V > 64$ voxels), for Anxious > Rest (A > R), Rest > Anxious (R > A), Neutral > Rest (N > R), and Rest > Neutral (R > N) contrasts.

Contrast	Tal coordinates	Anatomical region	Volume (in voxels)
Subject D			
A > R	[-27 -90 15]	Occipital Mid L, Calcarine L	396
	[34 -93 8]	Occipital Mid/Inf. R	246
R > A	[-10 -78 -6]	Lingual L, Calcarine L	217
N > R	[-26 -91 15]	Occipital Mid L	79
R > N	[12 -71 7]	Lingual L, Calcarine L	827
		Lingual R, Calcarine R	
		Precuneus R	
Subject T			
R > A	[4 -93 6]	Lingual L, Calcarine L	604
R > N	[-6 -65 12]	Lingual R, Calcarine R	682
		Lingual L, Calcarine L	
		Lingual R, Calcarine R	

while for Rest > Task, we found large clusters in the bilateral lingual and calcarine cortices, and, in D's case, in the precuneus.

3.1.2. Amygdala–prefrontal dynamics

We computed the cross correlation functions between the amygdala and the two prefrontal areas of our network (BA45 and BA9), shown in Figure 2. Since (as illustrated in Figure 1) the left and right ROI time series were very similar, we show here, for simplicity, the cross correlations using average bilateral time series for our regions (i.e., obtained by averaging the time series for the left and right hemisphere components of each individual region); the same functions calculated separately (for ipsilateral and contralateral time-series pairs) look very similar. Observing the small positive and negative lags may help us identify potential differences in HRF latencies in these regions between subjects or even understand the effects of causal connections between the two coupled regions. We noticed different trends in the two subjects. For example, while both D and T exhibit positive amygdala → BA45 correlations for small (2.1 s) lags, the converse BA45 → amygdala correlations are positive for D and negative for T for small (2.1 s) lags.

The amygdala and prefrontal cortex form excitatory and inhibitory components, respectively, of the negative feedback loop that regulates emotion. Therefore, increased amygdala activation subsequent to perception of stressful stimuli induces an overall excitatory effect on prefrontal regions, which in turn inhibit amygdala, contributing to fear extinction.

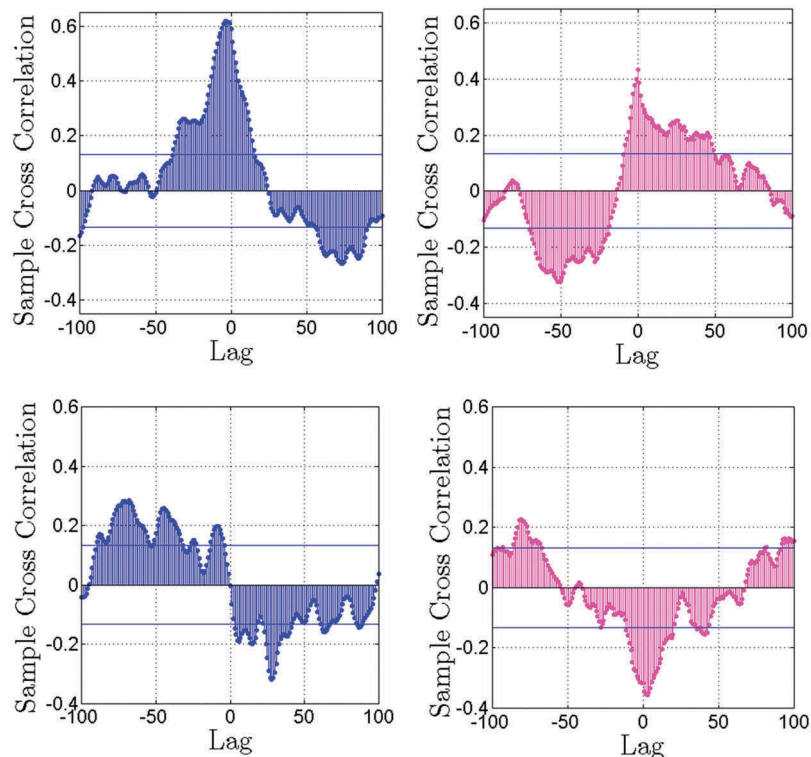


Figure 2. Cross correlation functions between amygdala and Brodmann Area 45 (top) and amygdala and Brodmann Area 9 (bottom), for subject D (left, in blue), and for T (right, in pink). The lag (unit along the x-axis) is 2.1 s. For positive lags, the values can be interpreted as amygdala → BA45 and amygdala → BA9 cross correlations, while for negative lags, the values represent BA45 → amygdala and BA9 → amygdala cross correlations. [To view this figure in color, please see the online version of this journal.]

The general belief has been that this prefrontal inhibition is implemented via excitatory PFC projections to GABA-ergic interneurons in the basolateral amygdala (BLA), which in turn massively inhibit other amygdala cells, leading to fear extinction. Newer studies suggest a more complex circuit such that the feedback arm of this regulatory loop is in fact composed of a few different pathways, with potentially opposite effects. For example, Likhtik, Pelletier, Paz, and Denis (2005) show that the overall excitatory effect of the prefrontal cortex on the amygdala is based on its activation of both pyramidal cells and interneurons in the BLA, possibly with different time scales. Moreover, the receptivity of the basolateral cells to prefrontal inhibition seems to depend on the strength of the amygdala to prefrontal feedforward projections. A different balance between the magnitude and timing of these effects may reflect in our directional cross-correlation results.

3.1.3. PC analysis

We performed a PC analysis, identifying the principal directions (eigenvectors) of the 12-dimensional phase space for each subject, and the spread (eigenvalue, or loading) in each of these directions. In our previous work, we have used this technique in combination with group statistical tools, to differentiate, based on trajectory geometry, between a group of schizophrenia patients and a group of healthy controls (Rădulescu & Mujica-Parodi, 2009).

We found that the loading values decay quite rapidly for both subjects so that only the leading PCs have a considerable contribution to the shape of the 12-dimensional trajectory (see Figure 3, and also Table 2). In the case of subject D, the first PC is almost five times larger in magnitude than the second one, suggesting that the contribution of the first PC is so strong in D's case that his trajectory is almost one-dimensional. In the case of subject T, the discrepancy between the two leading PCs is less dramatic, with the trajectory being almost completely contained in a two-dimensional plane.

We then located, in each case, the direction of the first PC, which captures most of the dynamic variability in the system. Table 3 shows the coefficients representing the contribution of each of the 12 variables (ROIs) to the leading PC vector. In D's case, the contribution of the amygdala is predominant,

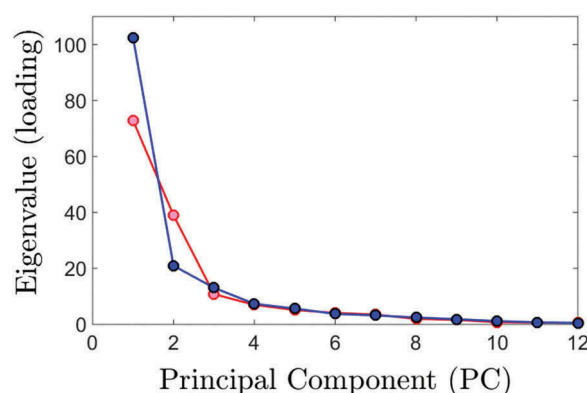


Figure 3. Loadings (eigenvalues) corresponding to the 12 principal components, for subject D (in dark blue) and for subject T (in light pink). The loading values decay very fast, suggesting that the 12-dimensional dynamics is in fact embedded in a lower dimensional subspace. [To view this figure in color, please see the online version of this journal.]

followed by the hippocampus and insula, while the prefrontal regions have clearly weaker contributions. In T's case, the contribution of the ROIs is much more balanced, with a slight predominance of the BA9 components. This reinforces the idea of T possessing unusually strong prefrontal control of the amygdala during an emotional task, while in D, the prefrontal control is less tight, allowing the normal arousal and extinction course in response to a stressor.

3.1.4. Exploratory power-spectral scale invariance

For each of the two subjects, we explored the whole brain, searching for voxels whose signals had a PSSI value β smaller than the threshold $\tau = -1.75$. In other words, we searched for the voxels with activity in the pink-brown noise range (showing markedly more structured signals in comparison with the rest of the active brain). Out of this subset of the brain, we retained only the contiguous clusters larger than $V = 27$ voxels (equivalent with the volume of a cube of side 3). The values of these parameters were finely tuned to best capture the relevant clusters, while trying to avoid possible random confounds. For each subject, we found four clusters with the required properties, characterized in Table 4, and also illustrated in Figure 4 for D, and in Figure 5 for T.

Table 2. Principal component characterization for subjects D and T.

		PC1	PC2	PC3	PC4	PC5	PC6	PC7	PC8	PC9	PC10	PC11	PC12
Loadings	D	102.4	20.9	13.0	7.3	5.6	3.7	3.2	2.4	1.8	1.1	0.7	0.5
	T	72.8	38.9	10.8	6.9	5.1	4.0	3.5	1.9	1.6	0.7	0.6	0.5

PC1–PC12 stand for the principal components of the system, arranged in the decreasing order of the eigenvalue magnitudes (loadings). In both cases, only the first PCs contribute significantly to the variability in the system, with a more pronounced relative spread in the direction of the first component in D's case (see also Figure 3).

Table 3. Principal component characterization for subjects D and T, in a network in which the variables are temporal activations in the right and left amygdala (RA and LA), right and left anterior cingulate cortex (LAC and RAC), right and left Brodmann Area 45 (RBA45 and LBA45), right and left Brodmann Area 9 (RBA9 and LBA9), left and right hippocampus (RH and LH), right insula and left insula (RI and LI).

		RA	LA	RAC	LAC	RBA45	LBA45	RBA9	LBA9	RH	LH	RI	LI
PC1 Coeff.	D	0.43	0.73	0.06	0.07	0.09	0.09	0.02	0.05	0.25	0.35	0.14	0.18
	T	0.25	0.22	0.39	0.42	0.28	0.28	0.38	0.36	0.15	0.14	0.18	0.15

The coefficients of the first principal component emphasize the different ROI contributions to the network dynamics in each case. For D, the predominant contributions are from the amygdala, hippocampus and insula, with comparatively minimal contributions from prefrontal regions and anterior cingulate. For T, the contributions are more uniform among all regions, with a slight dominance of prefrontal regions.

Table 4. Contiguous clusters larger than $V = 3^3$, whose voxels were identified to have $\beta < -1.75$, for subject D (top) and for subject T (bottom).

	Tal coordinates	Anatomical region	Volume (in voxels)
Subject D			
Cluster 1	[2 -89 1]	Calcarine L	44
Cluster 2	[-12 -75 7]	Calcarine R	93
Cluster 3	[-8 -72 46]	Precuneus L, R	235
Cluster 4	[44 -56 51]	Parietal Inf., Sup, Angular L	248
Subject T			
Cluster 1	[-42 -54 52]	Cerebellum R	36
Cluster 2	[6 -67 11]	Lingual L	72
Cluster 3	[-2 -66 46]	Precuneus L	57
Cluster 4	[-42 -54 52]	Parietal Sup, Angular R	41

The exploration not only found clusters in precuneus and parietal/angular cortex for both subjects but also two additional clusters in each case, situated in different regions for D and T.

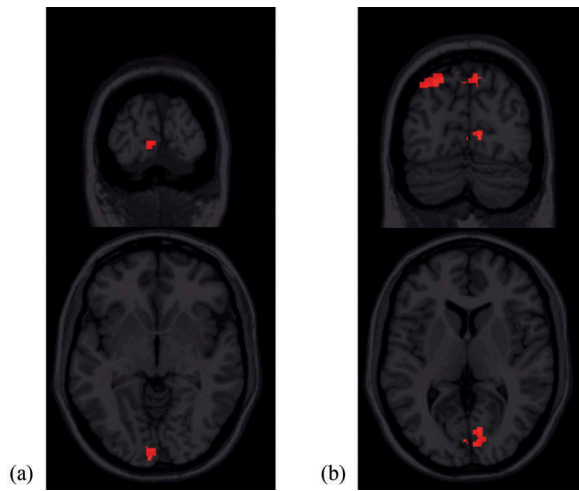


Figure 4. Subject D: illustration of contiguous voxel clusters of volume $V > 3^3$, with voxel-wise $\beta < -1.75$, as described in Table 4. (a) Coronal and axial view of Cluster 1 (calcarine). (b) Coronal view of Clusters 2, 3, and 4 (calcarine, precuneus, and parietal); axial view of Cluster 2 (calcarine).

While some clusters were different between the two subjects, the analysis also revealed two clusters situated for both D and T within the precuneus, and respectively in the superior parietal/angular cortex. One possible explanation may be that these clusters belong to a basic network that activates regardless of the emotional profile of the subject. A good candidate is the default mode network, which is known to include both precuneus and parietal regions, tightly linked with each other. In order to support the hypothesis of these clusters being specifically networked together, we computed, for each subject,

the average cross correlation coefficient, over all voxel pairs, for all pairs of clusters, and compared them with the average cross correlations of these clusters with the whole brain (all shown in Tables 5 and 6). The values show strongly pairwise-correlated signals within our cluster “network,” with p -values a few orders of magnitude smaller than the whole brain p -values, with the exception of Cluster 2 for T (Lingual), which is not as tightly correlated with Cluster 1 (cerebellum) and 4 (parietal).

We wanted to better understand and illustrate the differences between our two cases. For example, the two subjects’ regulatory networks could be tuned to different baselines so that regions of relative low efficiency within one subject may in fact correspond to a much higher relative efficiency in the other subject. We performed a direct comparison and searched specifically for the voxels with the most pronounced differences in β values between the two subjects (representing regions functioning at different efficiency levels in the two subjects, in response to identical conditions). We then compared these differences with the statistical differences found between the two subject groups to which D and T belonged, respectively.

More precisely, we looked for voxels for which the subject difference in β was larger in absolute value than $\tau = 1.5$ and imposed a cluster volume threshold of $V > 4^3$ contiguous voxels. We found seven clusters, labeled and described in Table 7: two cerebellar clusters with a positive $\beta_D - \beta_T$ difference (i.e., β values for D were closer to white noise than those for T), and five clusters with a negative $\beta_D - \beta_T$ difference (i.e., β values for T were closer to white noise); of these five clusters, four were situated in the superior frontal gyrus and dorsolateral prefrontal cortex (Brodmann Areas 6, 8, 9, 10, and 46), and one in a parietal region (in Brodmann Area 7).

3.2. Statistical results

We compared the voxel-wise PSSI between the low and high-reactivity groups and retained only the voxels with significantly different ($p < 0.01$) values of β , additionally imposing a cluster volume threshold of $V > 3^3$. We found two voxel clusters: the first, $V = 43$ voxels large, situated in the right frontal inferior orbital region and the second, $V = 44$ voxels large, situated in the right frontal superior region (Brodmann Area 10), as shown in Figure 8(a,b). An illustration of the distribution of β values within the first cluster is shown in Figure 8(c), with the values in the high-reactivity group closer to white noise than those in the low-reactivity group.

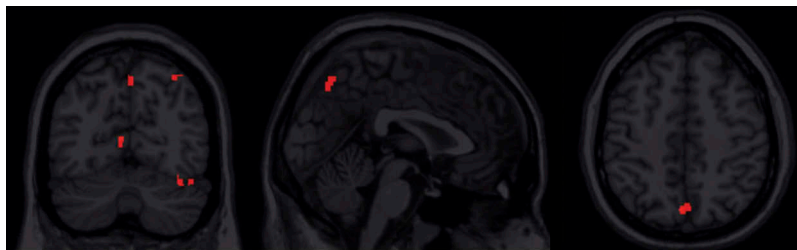


Figure 5. Subject T: illustration of contiguous voxel clusters of volume $V > 3^3$ with voxel-wise $\beta < -1.75$, as described in Table 4. Coronal view of all Clusters 1, 2, 3, and 4; sagittal view of Cluster 4 (parietal); axial view of Cluster 3 (precuneus).

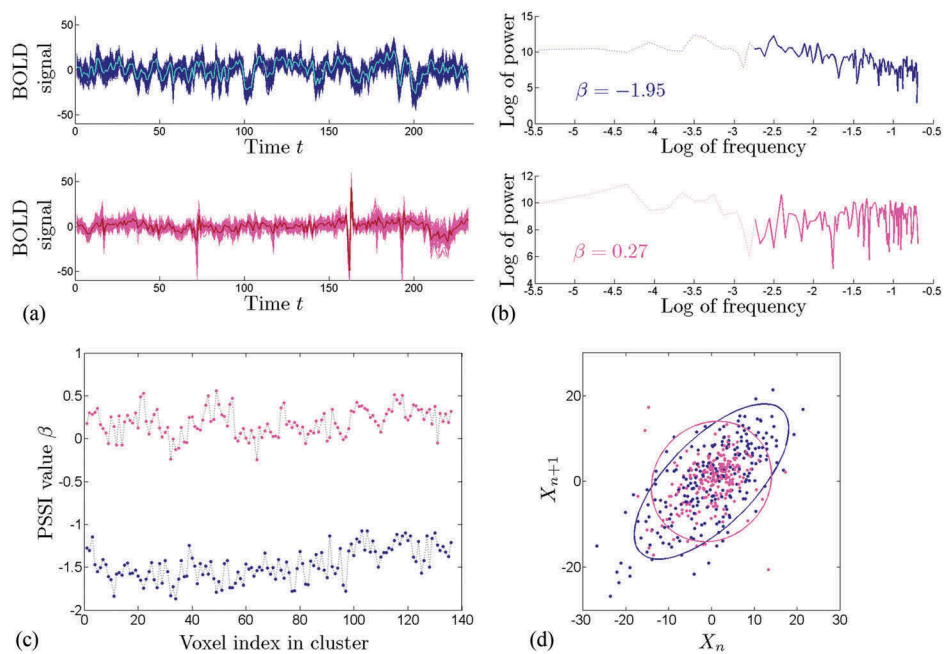


Figure 6. Description of Cluster 4 (left frontal superior medial). (a) Time series for all voxels in Cluster 4, for D (in dark blue) and for T (in light pink); cluster-wise average time series are shown in cyan (for D) and dark red (for T). (b) Cluster-wise PSSI β , calculated from the power spectrum density of the average cluster time series, shown in blue for D, and in pink for T. (c) Distribution of β values within the cluster voxels. The values for D are in the pink noise range (more structured), while those for T are within the white noise range (more chaotic). (d) Poincaré scatter plots, illustrating the variability differences between the cluster average signals of the two subjects: the principal directions are comparable between D and T, but the principal component ratio is larger for D (blue) than for T (red), suggesting a stronger preference/variability of D in the direction of its first PC. [To view this figure in color, please see the online version of this journal.]

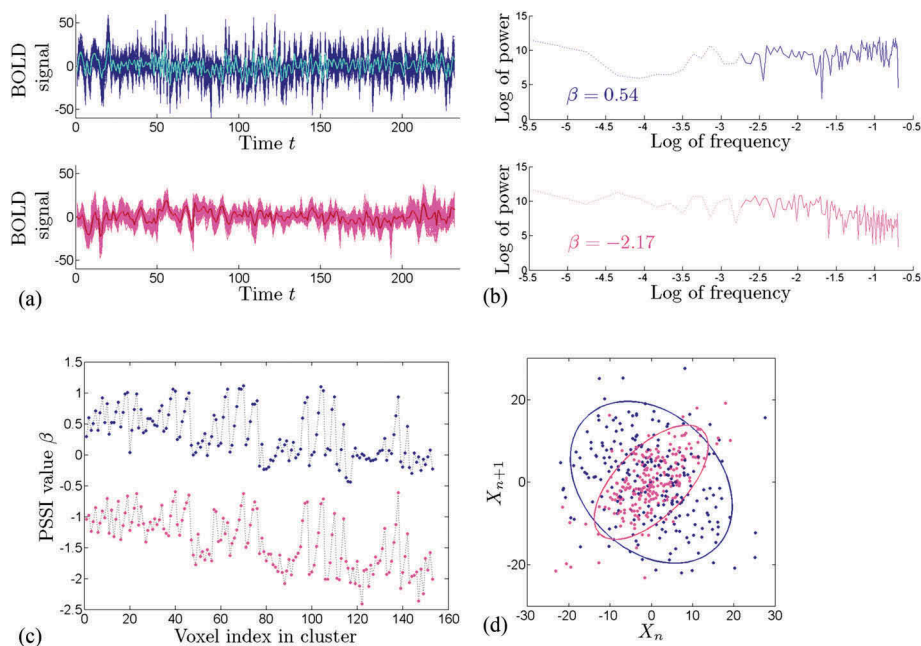


Figure 7. Description of Cluster 2 (left cerebellum). (a) Time series for all voxels in Cluster 2, for D (in dark blue) and for T (in light pink); cluster-wise average time series are shown in cyan (for D) and dark red (for T). (b) Cluster-wise PSSI β , calculated from the power spectrum density of the average cluster time series, shown in blue for D, and in red for T. (c) Distribution of β values within the cluster voxels. The values for D are in the white noise range (more chaotic), while those for T are within the pink noise range (higher efficiency), which is the opposite scenario than that encountered in Cluster 4. (d) Poincaré scatter plots, illustrating the variability differences between the cluster average signals of the two subjects: the first principal component of D is pointing in the direction of the second diagonal, perpendicular on that of T, suggesting larger jumps between consecutive points (higher variability). [To view this figure in color, please see the online version of this journal.]

Table 5. Subject D: Strength of cross correlation for each cluster pair, and between each cluster and the rest of the brain.

Subject D				
	Cluster 1	Cluster 2	Cluster 3	Cluster 4
Correlations between clusters: <i>R</i> values				
Cluster 1	0.85	0.73	0.65	0.37
Cluster 2	0.73	0.93	0.74	0.44
Cluster 3	0.65	0.74	0.82	0.52
Cluster 4	0.37	0.44	0.52	0.84
Correlations between clusters: <i>p</i> values				
Cluster 1	2.6×10^{-22}	3.9×10^{-14}	3.7×10^{-11}	10^{-4}
Cluster 2	3.9×10^{-14}	6.4×10^{-51}	1.5×10^{-16}	2×10^{-4}
Cluster 3	3.7×10^{-11}	1.5×10^{-16}	2.3×10^{-14}	6.7×10^{-5}
Cluster 4	10^{-4}	2×10^{-4}	6.7×10^{-5}	6×10^{-16}
Whole brain correlation values				
<i>R</i> values	0.25	0.36	0.29	0.23
<i>p</i> Values	0.09	0.07	0.08	0.1

Top: Average *R* values, computed for each cluster pair over all pairs of time series. Middle: Average pairwise *p* values. Bottom: Average *R* and *p* values, computed by pairing the cluster average time series with the time series corresponding to all other voxels in the active brain.

Table 6. Subject T: Strength of cross correlation for each cluster pair, and between each cluster and the rest of the brain.

Subject T				
	Cluster 1	Cluster 2	Cluster 3	Cluster 4
Correlations between clusters: <i>R</i> values				
Cluster 1	0.81	0.25	0.56	0.55
Cluster 2	0.25	0.90	0.46	0.19
Cluster 3	0.56	0.46	0.85	0.61
Cluster 4	0.55	0.19	0.61	0.83
Correlations between clusters: <i>p</i> values				
Cluster 1	4.3×10^{-15}	0.01	9.7×10^{-9}	1.8×10^{-6}
Cluster 2	0.01	10^{-39}	1.8×10^{-4}	0.08
Cluster 3	9.7×10^{-9}	1.8×10^{-4}	7×10^{-22}	3.1×10^{-7}
Cluster 4	1.8×10^{-6}	0.08	3.1×10^{-7}	10^{-13}
Whole brain correlation values				
	Cluster 1	Cluster 2	Cluster 3	Cluster 4
<i>R</i> values	0.34	0.37	0.26	0.39
<i>p</i> Values	0.07	0.06	0.09	0.06

Top: Average *R* values, computed for each cluster pair over all pairs of time series. Middle: Average pairwise *p* values. Bottom: Average *R* and *p* values, computed by pairing the cluster average time series with the time series corresponding to all other voxels in the active brain.

3.3. Second subject pair

We chose randomly two other individuals from our subject pool S2, with the only restriction based on their psycho-physiological measures: the first subject (which will be referred to

Table 8. Principal component characterization for subjects X and Y.

		PC1	PC2	PC3	PC4	PC5	PC6	PC7	PC8	PC9	PC10	PC11	PC12
Loadings	X	51.4	30.8	11.9	7.9	6.6	5.0	3.1	2.1	2.1	1.1	0.9	0.6
	Y	54.7	14.3	7.7	6.1	5.0	4.0	2.9	2.4	1.6	0.8	0.6	0.5

PC1–PC12 stand for the principal components of the system, arranged in the decreasing order of the eigenvalue magnitudes (loadings). In both cases, only the first PCs contribute significantly to the variability in the system (compare with Table 2).

Table 9. Principal component characterization for subjects X and Y, in a network in which the variables are temporal activations in the right and left amygdala (RA and LA), right and left anterior cingulate cortex (LAC and RAC), right and left Brodmann Area 45 (RBA45 and LBA45), right and left Brodmann Area 9 (RBA9 and LBA9), left and right hippocampus (RH and LH), right insula and left insula (RI and LI).

		RA	LA	RAC	LAC	RBA45	LBA45	RBA9	LBA9	RH	LH	RI	LI
PC1	X	0.36	0.73	0.02	0.00	0.11	0.30	0.17	0.11	0.17	0.29	0.14	0.18
Coeff.	Y	0.37	0.21	0.30	0.32	0.24	0.30	0.31	0.34	0.23	0.21	0.24	0.28

The coefficients of the first principal component emphasize the different ROI contributions to the network dynamics in each case (compare with Table 3).

Table 7. Clusters of largest differential PSSI, found via an exploratory search for contiguous volumes larger than $V = 4^3$ voxels, were β differs in absolute value by more than the threshold $\tau = 1.5$ between D and T.

Clusters with largest differential β (D–T)				
	Anatomical region	Brodman Area	Volume	Largest difference
Cluster 1	Cerebellum Crus1 L		153	2.19
Cluster 2	Cerebellum 4, 5 L		89	2.52
Cluster 3	Frontal Sup R	BA10	75	–2.06
Cluster 4	Frontal Sup Med L	BA10, BA46	136	–2.55
Cluster 5	Frontal Sup Med LR	BA8,BA9	123	–2.18
Cluster 6	Parietal Inf., Angular L		205	–2.34
Cluster 7	Frontal Mid, Precentral L	BA6	76	–2.22

The list includes two cerebellar regions where the D's signals were closer to white noise, while T's signals were in the brown noise range, as well as frontal and parietal regions with the opposite pattern. More detail for two representative clusters is illustrated in Figures 6 and 7.

as subject X) had a high trait anxiety score ($TA = 47$) and high average cortisol over the duration of the test ($Cor = 23.97$), suggesting high stress reactivity; the second (referred to as subject Y) had low trait anxiety ($TA = 28$) and a cortisol average reading almost 10 times lower ($Cor = 2.53$), suggesting low stress reactivity. For subjects X and Y, we performed the same analyses as for the original pair D and T.

The ROI-based PC analysis confirmed only the leading principal directions to be relevant to the time evolution, the loadings decaying very fast in the 12-dimensional space (see Table 8). The coefficients of the leading PC were found to be higher for left amygdala in the more stress reactive subject X, and generally higher for the anterior cingulate, prefrontal, and hippocampal regions for the less reactive subject Y (see Table 9). The values for Y are not as extreme as in the particularly stress nonreactive T, but the trend is clearly consistent with our first results.

We continued with the exploratory analysis, by searching in each subject for the clusters larger than $V = 3^3$ contiguous voxels with PSSI lower than $\beta = -1.75$. The results, shown in Table 10, confirm the involvement of visual regions in this primary auditory task (see Section 4), as well as the contributions from the precuneus and the parietal regions (which were detected by our analysis in both subjects X and Y). As before, for each subject, the average correlations between the time series within any pair of these clusters were found to be much higher than the average correlations of the clusters with the rest of the brain; the correlations between

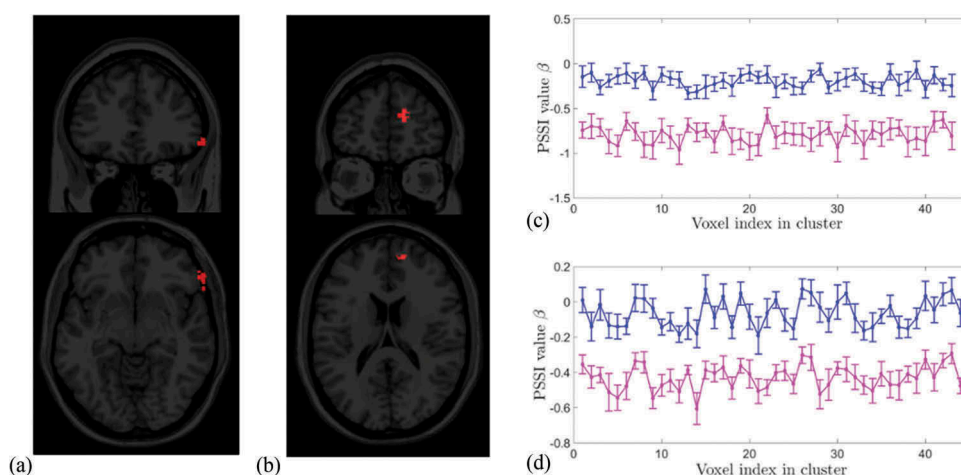


Figure 8. Clusters of significantly different PSSI between high and low reactivity groups ($p < 0.01$) found via an exploratory search for contiguous volumes larger than $V = 3^3$ voxels. Coronal and axial view of: (a) Cluster 1, $V = 43$, right frontal inferior orbital and (b) Cluster 2, $V = 44$, right frontal superior. (c) Distribution of group average β values within the Cluster 1 voxels, shown together with error bars. (d) Distribution of group average β values within the Cluster 2 voxels, shown together with error bars. The values for the low-reactivity group (in blue) are in the white noise range (more chaotic), while those for the high-reactivity group (in pink) are within the pink noise range (higher efficiency), which is the scenario supported by our existing ROI results, as well as by our current case study. [To view this figure in color, please see the online version of this journal.]

Table 10. Contiguous clusters larger than $V = 3^3$, whose voxels were identified to have $\beta < -1.75$, for subject X (top) and for subject Y (bottom).

	Tal coordinates	Anatomical region	Volume (in voxels)
Subject X			
Cluster 1	[16 -74 -6]	Cerebellum L	62
Cluster 2	[2 -91 16]	Calcarine L	163
Cluster 3	[-2 -67 51]	Precuneus L, R, Parietal Sup L	554
Cluster 4	[-4 -49 60]	Precuneus R	40
Cluster 5	[-34 -18 65]	Precentral R	30
Subject Y			
Cluster 1	[38 -71 -12]	Cerebellum L	28
Cluster 2	[20 -99 5]	Occipital, Calcarine L	75
Cluster 3	[-4 -85 12]	Calcarine R	50
Cluster 4	[38 -79 11]	Occipital Mid L	222
Cluster 5	[2 -82 23]	Cuneus L	54
Cluster 6	[-26 -84 23]	Occipital Mid R	58
Cluster 7	[48 -48 50]	Parietal Inf., Angular R	177
Cluster 8	[10 -67 57]	Precuneus L	38

The exploration not only found clusters in precuneus and parietal/angular cortex for both subjects but also additional clusters, situated in different regions for X and Y.

the precuneus and the parietal clusters were particularly strong. For example, in subject X, Clusters 3 and 4 are correlated with $p \sim 10^{-11}$, Clusters 4 and 5 with $p \sim 10^{-6}$, while Cluster 5 is not overall correlated with the rest of the brain ($p = 0.88$).

When comparing the two subjects directly (searching for clusters of size $V > 64$ voxels in which PSSI slopes differ between subjects by more than 1.5 in absolute value), we found a collection of 14 clusters, situated in the cerebellum, occipital, calcarine, temporal, precuneus, parietal, and frontal regions. Within the frontal cluster, the differences between the PSSI values for X and the corresponding ones for Y were found to be negative. This is consistent with our previous findings, with frontal slopes closer to white noise in the case of the less reactive subject Y and in the pink noise range for the more reactive subject X.

4. Discussion

In this study, we applied complexity measures of fMRI time series to case studies, in order to identify differences in functional efficiency at the single-subject level. Our results generally supported those obtained using more conventional techniques, such as the GLM, and statistical analyses of a larger subject group including two of the case studies. The complexity measures were, however, more sensitive in discriminating between subjects and identified additional patterns overlooked by the statistical tests. This suggests the value of complexity techniques when using imaging-derived quantitative measures for neurodiagnostic (single-subject level) applications.

It is interesting that both GLM and PSSI analyses identified areas with known function in visual processing (Allen, Buxton, Wong, & Courchesne, 1997; Macaluso, Frith, & Driver, 2000; Rockland & Ojima, 2003), although the task was primarily auditory. However, while the GLM in and of itself revealed activation in occipital, calcarine, and lingual cortices, it was the power-spectral analysis that may put these results in perspective, further relating functional efficiency in these areas to efficiency in frontal and parietal regions. This is important, since studies that have identified increased activity in the visual cortex in the absence of visual stimulation (Kastner, Pinsk, De Weerd, Desimone, & Ungerleider, 1999) had interpreted it as a top-down bias of neural signals in favor of the attended location, derived from a fronto-parietal network (which showed an even stronger signal increase during the auditory expectation than did visual areas).

While the calcarine sulcus has a more primary visual function (Rockland & Ojima, 2003), lingual areas seem to play a different role in vision, having been related to processing of complex images and written language (Price, 2000), encoding of visual memories and daydreaming (Dresler et al., 2014; Hölzel et al., 2007). Involvement of lingual areas suggests a higher level of cognitive processing during the anticipation

periods, which may relate to the subject's ability to inhibit emotional arousal.

Our prior group ROI analyses (Mujica-Parodi et al., 2014), further centralized and interpreted in our modeling work (Rădulescu, 2014), revealed prefrontal signals closer to white noise in more stress-nonreactive individuals as compared to healthy controls. Our current exploratory statistics supports these results: both significant clusters found by the statistical comparison between the low and high-reactivity groups were in frontal regions, with signals significantly closer to white noise in the highly nonreactive individuals. The single-subject results in frontal/prefrontal areas are in line with the statistics. We found that T (the stress resilient subject in the first pair) had flatter spectra than D in two of the clusters identified by the analysis, situated in the frontal cortex. Notice the consistency with Y, the stress resilient subject in the second pair, also showing flatter spectra than X in the one frontal cluster identified by the analysis of this pair. Hence, both case study comparisons supported the statistical results, in that stress resilience was associated with more chaotic (i.e., closer to white noise) frontal/prefrontal time series. Recall that $\beta \sim 0$ in the prefrontal cortex can be interpreted as increased efficiency of the inhibitory component of the fear response in nonreactive subjects. Note that the other clusters (e.g., situated in the cerebellum and parietal cortex) showed an opposite effect (with D's signals closer to white noise, and T's signals in the optimal pink noise range).

The single-subject analysis further suggested that, beyond clear overlaps, the network recruited during the anticipation task may be different and/or differently regulated between two individuals. First, our PC decomposition found different predominant directions in the subjects' phase space, supporting the idea of a higher amygdala contribution to dynamics in the case of D and X – leading to higher sensitivity to the anticipation stimuli, and a stronger arousal response to stressors – and a higher contribution from frontal regions (in the case of T), as well as anterior cingulate and hippocampus regions (in the case of Y) – leading to stronger inhibitory control, and higher stress resilience.

The idea was supported by the PSSI voxel differences found by our exploration, which identified networks of clusters with both similarities and differences between the two subjects. For example, clusters in the posterior (visual) and central (associative) precuneus and the superior parietal/angular cortex were found to have signals close to brown noise in both subjects, implying that these regions operate with high efficiency in both subjects. The precuneus and the parietal cortex are both well known as parts of the default mode network. The precuneus has been related to self-referential processing, imagery and memory, and more recently to aversive conditioning (Pizzagalli, Greischar, & Davidson, 2003). New hypotheses suggest that these functional aspects can be explained on the basis of the high centrality of the precuneus in the cortical network. Olaf Sporns and Ed Bullmore have proposed that the precuneus has a crucial role as a central and well connected “small-world network” hub between parietal and prefrontal regions (Bullmore & Sporns, 2009), which are interlinked by specialized hub regions, ensuring that overall path lengths across the network are short. Our current findings (very high

cross-correlation coefficients between the precuneus and parietal clusters in both subjects) are in line with this theory.

In addition to these regions common to all subjects, we also identified regions operating at significantly different efficiency levels between the two individuals in each pair. To fix our ideas, we will focus primarily on further interpreting the results for our first pair and only briefly discuss and draw comparisons with the second pair. This can be seen as an example of how this type of analysis may provide subject-customized information on brain regulation efficiency, as well as means of targeting the sources of behavioral differences between two individuals.

For example, D showed additional involvement of calcarine areas (tightly correlated with the precuneus and the parietal clusters, as previously discussed), while for T our analysis identified two clusters in the cerebellum and the lingual gyrus. These differences were also identified by our analysis within the second subject pair, although not as prominent as for D–T. (This was to be expected, given the less dramatic behavioral differences between X and Y.)

Our results are consistent with recent theories of the involvement of cerebellar areas in higher cognitive processing and neural computation. The cerebellum has been long thought to play its most important role in motor control (Fine, Ionita, & Lohr et al., 2002; Houk, Buckingham, & Barto, 1996), but recent studies have found it to also be crucially involved in cognitive functions such as attention and language (Rapp, 2001), and in the regulation of fear and pleasure responses (Turner et al., 2007). It has been argued that the function of the cerebellum is best understood in terms of what neural computations it performs as a device for supervised learning (Doya, 2000). This may provide an explanation for the fact that, in our case, subject T, with tighter emotional control when anticipating aversive stimuli, was also the subject showing a more efficient regulation of cerebellar areas recruited during the anticipation: when searching for direct differences between D and T, we found two cerebellar clusters with β values for T significantly smaller than those for D (i.e., a cluster-average $\beta \sim 0$ for D and $\beta \sim -2$ for T).

The most important differences between subjects D and T were those reported in prefrontal regions, where the β values for T were close to white noise, while for D, they were in the brown noise range ($\beta \sim -2$). These results are significant in a few ways. First, they suggest that the cerebellum and the prefrontal cortex, while both being hypothesized to contribute to emotional regulation, do so by different mechanisms and with different effects [e.g., the cerebellum is believed to perform supervised learning, while the cerebral cortex performs unsupervised learning (Doya, 2000)].

Second, the results in Brodmann Areas 9 and 10 agree very well with our previous statistical results on emotional regulation. In group analyses applied to a few of our datasets, we have found the dorsolateral prefrontal cortex to be involved in emotional regulation. Symptoms of general anxiety were further correlated with decreased Brodmann Area 9 efficiency in inhibiting arousal (Carlson et al., 2011; Tolkunov et al., 2010), while symptoms of schizophrenia were associated with sub-optimal responses in both Brodmann Areas 9 and 10 (Rădulescu & Mujica-Parodi, 2009, 2008).

The most prominent differences in prefrontal efficiency between the two subjects appeared, however, in Brodmann Areas 6, 8, and 46, areas which had not previously identified by our group analyses, but which all support the idea of exacerbated prefrontal control in the stress resilient subject T during the anticipation task. The superior frontal gyrus (Brodmann Area 6) is a known premotor area (Chouinard & Paus, 2006), shown to activate “in preparation for action” during tasks such as anticipation of object properties (Schubotz & Yves Von Cramon, 2001) or of reward (Ernst et al., 2004). Brodmann Area 8 is involved in the management of uncertainty (Volz, Schubotz, & Cramon, 2005). Differences found in the Brodmann Area 46 may suggest underlying differences in sustaining attention and working memory (Courtney, Petit, Maisog, Ungerleider, & Haxby, 1998; Petrides, 2000), through the involvement of the dorsolateral prefrontal cortex in judgments about input relevance. Recent studies relating stimulation of BA46 with efficient treatment of depression (Fox, Buckner, White, Greicius, & Alvaro, 2012) have strengthened the evidence of its ties with emotional regulation mechanisms (Siegle, Thompson, Carter, Steinhauer, & Thase, 2007).

Overall, the results for our second subject pair showed similar basic trends and differences between emotional reactivity types as in the case of our original pair, with the variability that one would naturally expect to find between different individuals. Importantly, these clusters had failed to be detected by the same measures when used in conjunction with group statistics, although our current findings are qualitatively replicable between single subjects. This suggests once more the importance of using single-subject methods to support traditional statistical analyses when interpreting imaging data for clinical decisions on specific individuals.

A limitation of this study is that it illustrates scale-free properties of brain signals in a univariate, rather than multivariate setting. There is increasing supporting evidence that estimating the amount of fractality (and its fluctuations from rest to task) is more accurate in the latter setting (Pellé et al., 2016). Our future studies on scale-free dynamics from fMRI data will focus on computing multifractal measures of spatially regularized signals, to compensate for their shortness in time. Future work will also address other datasets and perform a more systematic set of comparisons to ensure that this type of results is independent of the task and consistent for many subject pairs.

Acknowledgments

We would like to thank Dr. Lilianne Mujica-Parodi and the Laboratory for Computational Neurodiagnostics for providing the subject data, and Ms. Sanja Nedic for the helpful discussions.

Disclosure statement

No potential conflict of interest was reported by the authors.

References

- Allen, G., Buxton, R. B., Wong, E. C., & Courchesne, E. (1997). Attentional activation of the cerebellum independent of motor involvement. *Science*, 275, 1940–1943. doi:10.1126/science.275.5308.1940
- Anderson, J. S., Zielinski, B. A., Nielsen, J. A., & Ferguson, M. A. (2014). Complexity of low-frequency blood oxygen level-dependent fluctuations covaries with local connectivity. *Human Brain Mapping*, 35, 1273–1283. doi:10.1002/hbm.22251
- Bandettini, P. A., et al. (2008). Endogenous oscillations and networks in functional magnetic resonance imaging. *Human Brain Mapping*, 29, 737. doi:10.1002/hbm.20607
- Banks, S. J., Eddy, K. T., Angstadt, M., Nathan, P. J., & Phan, K. L. (2007). Amygdala–frontal connectivity during emotion regulation. *Social Cognitive and Affective Neuroscience*, 2, 303–312. doi:10.1093/scan/nsm029
- Barnes, A., Bullmore, E. T., & Suckling, J. (2009). Endogenous human brain dynamics recover slowly following cognitive effort. *Plos One*, 4, e6626. doi:10.1371/journal.pone.0006626
- Bassett, D. S., & Gazzaniga, M. S. (2011). Understanding complexity in the human brain. *Trends in Cognitive Sciences*, 15, 200–209. doi:10.1016/j.tics.2011.03.006
- Bédard, C., & Destexhe, A. (2009). Macroscopic models of local field potentials and the apparent 1/f noise in brain activity. *Biophysical Journal*, 96, 2589–2603. doi:10.1016/j.bpj.2008.12.3951
- Bianciardi, M., Fukunaga, M., Van Gelderen, P., Horovitz, S. G., De Zwart, J. A., & Duyn, J. H. (2009). Modulation of spontaneous fmri activity in human visual cortex by behavioral state. *Neuroimage*, 450, 160–168. doi:10.1016/j.neuroimage.2008.10.034
- Boustani, S. E., Marre, O., Béhuret, S., Baudot, P., Yger, P., Bal, T., ... Yves, F. (2009). Network-state modulation of power-law frequency-scaling in visual cortical neurons. *Plos Comput Biol*, 5, e1000519. doi:10.1371/journal.pcbi.1000519
- Büchel, C., & Friston, K. J. (1997). Modulation of connectivity in visual pathways by attention: Cortical interactions evaluated with structural equation modelling and fmri. *Cerebral Cortex*, 7, 768–778. doi:10.1093/cercor/7.8.768
- Bullmore, E., Barnes, A., Bassett, D. S., Fornito, A., Kitzbichler, M., Meunier, D., & Suckling, J. (2009). Generic aspects of complexity in brain imaging data and other biological systems. *Neuroimage*, 47, 1125–1134. doi:10.1016/j.neuroimage.2009.05.032
- Bullmore, E., Long, C., Suckling, J., Fadili, J., Calvert, G., Zelaya, F., ... Brammer, M. (2001). Colored noise and computational inference in neurophysiological (fmri) time series analysis: Resampling methods in time and wavelet domains. *Human Brain Mapping*, 12, 61–78. doi:10.1002/(ISSN)1097-0193
- Bullmore, E., & Sporns, O. (2009). Complex brain networks: Graph theoretical analysis of structural and functional systems. *Nature Reviews Neuroscience*, 10, 186–198. doi:10.1038/nrn2575
- Buzsáki, G. (2006). *Rhythms of the Brain*. New York, NY: Oxford University Press.
- Carlson, J. M., Greenberg, T., Rubin, D., & Mujica-Parodi, L. R. (2011). Feeling anxious: Anticipatory amygdalo-insular response predicts the feeling of anxious anticipation. *Social Cognitive and Affective Neuroscience*, 6, 74–81. doi:10.1093/scan/nsq017
- Chatterjee, A. (2005). A madness to the methods in cognitive neuroscience?. *Journal of Cognitive Neuroscience*, 17, 847–849. doi:10.1162/0898929054021085
- Chouinard, P. A., & Paus, T. (2006). The primary motor and premotor areas of the human cerebral cortex. *The Neuroscientist*, 12, 143–152. doi:10.1177/1073858405284255
- Ciuciu, P., Abry, P., & He, B. J. (2014). Interplay between functional connectivity and scale-free dynamics in intrinsic fmri networks. *Neuroimage*, 95, 248–263. doi:10.1016/j.neuroimage.2014.03.047
- Ciuciu, P., Varoquaux, G., Abry, P., Sadaghiani, S., & Kleinschmidt, A. (2012). Scale-free and multifractal time dynamics of fMRI signals during rest and task. *Frontiers in Physiology*, 3, 186–186. doi:10.3389/fphys.2012.00186
- Courtney, S. M., Petit, L., Maisog, J. M., Ungerleider, L. G., & Haxby, J. V. (1998). An area specialized for spatial working memory in human frontal cortex. *Science*, 279, 1347–1351. doi:10.1126/science.279.5355.1347

- Culham, J. C. (2006). Functional neuroimaging: Experimental design and analysis. *Handbook of Functional Neuroimaging of Cognition*, 2, 53–82.
- Danckert, J., Mirsattari, S. M., & Bright, P. (2012). *Neuroimaging of single cases: Benefits and pitfalls*. InTech Europe Open Access Publisher.
- Daneshyari, M., Lily Kamkar, L., & Daneshyari, M. (2010). Epileptic EEG: A comprehensive study of nonlinear behavior. In: Arabnia H. (eds) *Advances in Computational Biology. Advances in Experimental Medicine and Biology*, 680: 677-683. New York, NY: Springer.
- Doya, K. (2000). Complementary roles of basal ganglia and cerebellum in learning and motor control. *Current Opinion in Neurobiology*, 10, 732–739. doi:10.1016/S0959-4388(00)00153-7
- Dresler M, Wehrle R, Spormaker V, Steiger A, Holsboer F, Czisch M, Hobson JA (2015). Neural correlates of insight in dreaming and psychosis. In *Sleep Medicine Reviews*, 20, 92-99. Elsevier.
- Engoren, M. (1998). Approximate entropy of respiratory rate and tidal volume during weaning from mechanical ventilation. *Critical Care Medicine*, 26, 1817–1823. doi:10.1097/00003246-199811000-00021
- Ernst, M., Nelson, E.E., McClure, E.B., Monk, C.S., Munson, S., Eshel, N., Zarahn, E., Leibenluft, E., Zametkin, A., Towbin, K. and Blair, J. (2004). Choice selection and reward anticipation: An fMRI study. *Neuropsychologia*, 42, 1585–1597. doi:10.1016/j.neuropsychologia.2004.05.011
- Etkin, A., Egner, T., & Kalisch, R. (2011). Emotional processing in anterior cingulate and medial prefrontal cortex. *Trends in Cognitive Sciences*, 15, 85–93. doi:10.1016/j.tics.2010.11.004
- Fine EJ, Ionita CC, Lohr L (2002). The history of the development of the cerebellar examination. In *Seminars in Neurology*, 22 (4) 375-384. New York, NY: Thieme Medical Publishers.
- Fox, M. D., Buckner, R. L., White, M. P., Greicius, M. D., & Alvaro, P.-L. (2012). Efficacy of transcranial magnetic stimulation targets for depression is related to intrinsic functional connectivity with the subgenual cingulate. *Biological Psychiatry*, 72, 595–603. doi:10.1016/j.biopsych.2012.04.028
- Fransson, P. (2006). How default is the default mode of brain function?: Further evidence from intrinsic bold signal fluctuations. *Neuropsychologia*, 44, 2836–2845. doi:10.1016/j.neuropsychologia.2006.06.017
- Fransson, P., Metsäranta, M., Blennow, M., Åden, U., Lagercrantz, H., & Vanhatalo, S. (2013). Early development of spatial patterns of power-law frequency scaling in fmri resting-state and eeg data in the newborn brain. *Cerebral Cortex*, 23, 638–646. doi:10.1093/cercor/bhs047
- Freyer, F., Aquino, K., Robinson, P. A., Ritter, P., & Breakspear, M. (2009). Bistability and non-gaussian fluctuations in spontaneous cortical activity. *The Journal of Neuroscience*, 29, 8512–8524. doi:10.1523/JNEUROSCI.0754-09.2009
- Friston, K. J., Harrison, L., & Penny, W. (2003). Dynamic causal modelling. *Neuroimage*, 19, 1273–1302. doi:10.1016/S1053-8119(03)00202-7
- Friston, K. J., & Price, C. J. (2003). Degeneracy and redundancy in cognitive anatomy. *Trends in Cognitive Sciences*, 7, 151–152. doi:10.1016/S1364-6613(03)00054-8
- Glenn, T., Whybrow, P. C., Rasgon, N., Grof, P., Alda, M., Baethge, C., & Bauer, M. (2006). Approximate entropy of self-reported mood prior to episodes in bipolar disorder. *Bipolar Disorders*, 8, 424–429. doi:10.1111/j.1399-5618.2006.00373.x
- Goldin, P. R., McRae, K., Ramel, W., & Gross, J. J. (2008). The neural bases of emotion regulation: Reappraisal and suppression of negative emotion. *Biological Psychiatry*, 63, 577–586. doi:10.1016/j.biopsych.2007.05.031
- He, B. J. (2011). Scale-free properties of the functional magnetic resonance imaging signal during rest and task. *The Journal of Neuroscience*, 31, 13786–13795. doi:10.1523/JNEUROSCI.2111-11.2011
- He, B. J. (2014). Scale-free brain activity: Past, present, and future. *Trends in Cognitive Sciences*, 18, 480–487. doi:10.1016/j.tics.2014.04.003
- He, B. J., & Raichle, M. E. (2009). The fMRI signal, slow cortical potential and consciousness. *Trends in Cognitive Sciences*, 13, 302–309. doi:10.1016/j.tics.2009.04.004
- He, B. J., Zempel, J. M., Snyder, A. Z., & Raichle, M. E. (2010). The temporal structures and functional significance of scale-free brain activity. *Neuron*, 66, 353–369. doi:10.1016/j.neuron.2010.04.020
- Hölzel, B. K., Ott, U., Hempel, H., Hackl, A., Wolf, K., Stark, R., & Vaitl, D. (2007). Differential engagement of anterior cingulate and adjacent medial frontal cortex in adept meditators and non-meditators. *Neuroscience Letters*, 421, 16–21. doi:10.1016/j.neulet.2007.04.074
- Houk, J. C., Buckingham, J. T., & Barto, A. G. (1996). Models of the cerebellum and motor learning. *Behavioral and Brain Sciences*, 19, 368–383. doi:10.1017/S0140525X00081474
- Huff, D. (1954). *How to lie with statistics*. New York, NY : W.W. Norton & Company.
- Huikuri, H. V., Mäkikallio, T. H., Peng, C.-K., Goldberger, A. L., Hintze, U., Möller, M., et al. (2000). Fractal correlation properties of R-R interval dynamics and mortality in patients with depressed left ventricular function after an acute myocardial infarction. *Circulation*, 101, 47–53. doi:10.1161/01.CIR.101.1.47
- Ide, J. S., Sien, H., Zhang, S., Mujica-Parodi, L. R., & Li Chiang-Shan, R. (2016). Power spectrum scale invariance as a neural marker of cocaine misuse and altered cognitive control. *Neuroimage: Clinical*, 11, 349–356. doi:10.1016/j.nicl.2016.03.004
- Kastner, S., Pinsk, M. A., De Weerd, P., Desimone, R., & Ungerleider, L. G. (1999). Increased activity in human visual cortex during directed attention in the absence of visual stimulation. *Neuron*, 22, 751–761. doi:10.1016/S0896-6273(00)80734-5
- Kim, J., Zhu, W., Chang, L., Bentler, P. M., & Ernst, T. (2007). Unified structural equation modeling approach for the analysis of multisubject, multivariate functional mri data. *Human Brain Mapping*, 28, 85–93. doi:10.1002/hbm.20259
- Lai M-C, Lombardo MV, Chakrabarti B, Sadek SA, Pasco G, Wheelwright SJ, Bullmore ET, Baron-Cohen S, Suckling J, MRC AIMS Consortium. (2010). A shift to randomness of brain oscillations in people with autism. *Biological Psychiatry*, 68, 1092–1099. doi:10.1016/j.biopsych.2010.06.027
- Levina, A., Michael Herrmann, J., & Geisel, T. (2007). Dynamical synapses causing self-organized criticality in neural networks. *Nature Physics*, 3, 857–860. doi:10.1038/nphys758
- Likhtik, E., Pelletier, J. G., Paz, R., & Denis, P. (2005). Prefrontal control of the amygdala. *The Journal of Neuroscience*, 25, 7429–7437. doi:10.1523/JNEUROSCI.2314-05.2005
- Lowen, S. B., Cash, S. S., Poo, M.-M., & Teich, M. C. (1997). Quantal neurotransmitter secretion rate exhibits fractal behavior. *The Journal of Neuroscience*, 17, 5666–5677.
- Macaluso, E., Frith, C. D., & Driver, J. (2000). Modulation of human visual cortex by crossmodal spatial attention. *Science*, 289, 1206–1208. doi:10.1126/science.289.5482.1206
- Maxim, V., Şendur, L., Fadili, J., Suckling, J., Gould, R., Howard, R., & Bullmore, E. D. (2005). Fractional Gaussian noise, functional MRI and Alzheimer's disease. *Neuroimage*, 25, 141–158. doi:10.1016/j.neuroimage.2004.10.044
- Montano, N., Gnechi Ruscone, T., Porta, A., Lombardi, F., Pagani, M., & Malliani, A. (1994). Power spectrum analysis of heart rate variability to assess the changes in sympathovagal balance during graded orthostatic tilt. *Circulation*, 90, 1826–1831. doi:10.1161/01.CIR.90.4.1826
- Mujica-Parodi, L. R., Carlson, J. M., Cha, J., & Rubin, D. (2014). The fine line between brave and reckless: Amygdala reactivity and regulation predict recognition of risk. *NeuroImage*. doi:10.1016/j.neuroimage.2014.08.038
- Mujica-Parodi, L. R., Korgaonkar, M., Ravindranath, B., Greenberg, T., Tomasi, D., Wagshul, M., ... Zhong, Y., et al. (2009). Limbic dysregulation is associated with lowered heart rate variability and increased trait anxiety in healthy adults. *Human Brain Mapping*, 30, 47–58. doi:10.1002/hbm.20483
- Nedic, S., Stufflebeam, S. M., Rondinoni, C., Velasco, T. R., Antonio, C. D. S., Leite, J. P., ... Ide, J. S. (2015). Using network dynamic fMRI for detection of epileptogenic foci. *BMC Neurology*, 15, 1. doi:10.1186/s12883-015-0514-y
- Ochsner, K. N., Ray, R. D., Cooper, J. C., Robertson, E. R., Chopra, S., Gabrieli, J. D. E., & Gross, J. J. (2004). For better or for worse: Neural systems supporting the cognitive down-and up-regulation of negative emotion. *Neuroimage*, 23, 483–499. doi:10.1016/j.neuroimage.2004.06.030
- Paulus, M. P., Geyer, M. A., & Braff, D. L. (1996). Use of methods from chaos theory to quantify a fundamental dysfunction in the behavioral organization of schizophrenic patients. *The American Journal of Psychiatry*, 153, 714. doi:10.1176/ajp.153.5.714
- Pellé, H., Ciucci, P., Rahim, M., Dohmatob, E., Abry, P., & Wassenhove, V. V. Multivariate hurst exponent estimation in fMRI. Application to brain

- decoding of perceptual learning. In *Biomedical Imaging (ISBI), 2016 IEEE 13th International Symposium on*, pages 996–1000. IEEE, 2016.
- Petrides, M. (2000). The role of the mid-dorsolateral prefrontal cortex in working memory. In *Experimental Brain Research*, 133, 44–54. Springer.
- Pezard, L., Nandrino, J.-L., Renault, B., Massiou, F. E., Allilaire, J.-F., Müller, J., ... Martinerie, J. (1996). Depression as a dynamical disease. *Biological Psychiatry*, 39, 991–999. doi:10.1016/0006-3223(95)00307-X
- Phelps, E. A. (2004). Human emotion and memory: Interactions of the amygdala and hippocampal complex. *Current Opinion in Neurobiology*, 14, 198–202. doi:10.1016/j.conb.2004.03.015
- Phelps, E. A., & LeDoux, J. E. (2005). Contributions of the amygdala to emotion processing: From animal models to human behavior. *Neuron*, 48, 175–187. doi:10.1016/j.neuron.2005.09.025
- Pincus, S., & Singer, B. H. (1996). Randomness and degrees of irregularity. *Proceedings of the National Academy of Sciences*, 93, 2083–2088. doi:10.1073/pnas.93.5.2083
- Pincus, S. M. (1991). Approximate entropy as a measure of system complexity. *Proceedings of the National Academy of Sciences*, 88, 2297–2301. doi:10.1073/pnas.88.6.2297
- Pincus, S. M. (2003). Quantitative assessment strategies and issues for mood and other psychiatric serial study data. *Bipolar Disorders*, 5, 287–294. doi:10.1034/j.1399-5618.2003.00036.x
- Pincus, S. M. (2006). Approximate entropy as a measure of irregularity for psychiatric serial metrics. *Bipolar Disorders*, 8, 430–440. doi:10.1111/j.1399-5618.2006.00375.x
- Pincus, S. M., & Goldberger, A. L. (1994). Physiological time-series analysis: What does regularity quantify?. *American Journal of Physiology-Heart and Circulatory Physiology*, 266, H1643–H1656.
- Pizzagalli, D. A., Greischar, L. L., & Davidson, R. J. (2003). Spatio-temporal dynamics of brain mechanisms in aversive classical conditioning: High-density event-related potential and brain electrical tomography analyses. *Neuropsychologia*, 41, 184–194. doi:10.1016/S0028-3932(02)00148-3
- Price, C. J. (2000). The anatomy of language: Contributions from functional neuroimaging. *Journal of Anatomy*, 197, 335–359. doi:10.1046/j.1469-7580.2000.19730335.x
- Radhakrishnan, N., & Gangadhar, B. N. (1998). Estimating regularity in epileptic seizure time-series data. *IEEE Engineering in Medicine and Biology Magazine*, 17, 89–94. doi:10.1109/51.677174
- Rădulescu, A., & Mujica-Parodi, L. R. (2014). Network connectivity modulates power spectrum scale invariance. *Neuroimage*, 90(436–448). doi:10.1016/j.neuroimage.2013.12.001
- Rădulescu, A. R., & Mujica-Parodi, L. R. (2008). A systems approach to prefrontal-limbic dysregulation in schizophrenia. *Neuropsychobiology*, 57, 206–216. doi:10.1159/000151731
- Rădulescu, A. R., & Mujica-Parodi, L. R. (2009). A principal component network analysis of prefrontal-limbic functional magnetic resonance imaging time series in schizophrenia patients and healthy controls. *Psychiatry Research: Neuroimaging*, 174, 184–194. doi:10.1016/j.psychres.2009.04.017
- Rădulescu, A. R., Rubin, D., Strey, H. H., & Mujica-Parodi, L. R. (2012). Power spectrum scale invariance identifies prefrontal dysregulation in paranoid schizophrenia. *Human Brain Mapping*, 33, 1582–1593. doi:10.1002/hbm.21309
- Rapp, B. (2001). *The handbook of cognitive neuropsychology: What deficits reveal about the human mind*. Psychology Press.
- Rockland, K. S., & Ojima, H. (2003). Multisensory convergence in calcarine visual areas in macaque monkey. *International Journal of Psychophysiology*, 50, 19–26. doi:10.1016/S0167-8760(03)00121-1
- Roebroeck, A., Formisano, E., & Goebel, R. (2005). Mapping directed influence over the brain using Granger causality and fMRI. *Neuroimage*, 25, 230–242. doi:10.1016/j.neuroimage.2004.11.017
- Roelfsema, F., Pincus, S. M., & Veldhuis, J. D. (1998). Patients with cushings disease secrete adrenocorticotropin and cortisol jointly more asynchronously than healthy subjects. *The Journal of Clinical Endocrinology & Metabolism*, 83, 688–692.
- Rubin, D., Fekete, T., & Mujica-Parodi, L. R. (2013). Optimizing complexity measures for fMRI data: Algorithm, artifact, and sensitivity. *Plos One*, 8, e63448. doi:10.1371/journal.pone.0063448
- Rubin, M., Sporns, O., Thivierge, J.-P., & Breakspear, M. (2011). Neurobiologically realistic determinants of self-organized criticality in networks of spiking neurons. *Plos Comput Biol*, 7, e1002038. doi:10.1371/journal.pcbi.1002038
- Ryan, S. M., Goldberger, A. L., Pincus, S. M., Mietus, J., & Lipsitz, L. A. (1994). Gender-and age-related differences in heart rate dynamics: Are women more complex than men?. *Journal of the American College of Cardiology*, 24, 1700–1707. doi:10.1016/0735-1097(94)90177-5
- Schaefer, A., Brach, J. S., Perera, S., & Ervin, S. (2014). A comparative analysis of spectral exponent estimation techniques for 1/f β processes with applications to the analysis of stride interval time series. *Journal of Neuroscience Methods*, 222, 118–130. doi:10.1016/j.jneumeth.2013.10.017
- Schmitz, O., Porksen, N., Nyholm, B., Skjærbaek, C., Butler, P. C., Veldhuis, J. D., & Pincus, S. M. (1997). Disorderly and nonstationary insulin secretion in relatives of patients with niddm. *American Journal of Physiology-Endocrinology and Metabolism*, 272, E218–E226.
- Schubotz, R. I., & Yves Von Cramon, D. (2001). Functional organization of the lateral premotor cortex: fMRI reveals different regions activated by anticipation of object properties, location and speed. *Cognitive Brain Research*, 11, 97–112. doi:10.1016/S0926-6410(00)00069-0
- Shimizu, Y., Barth, M., Windischberger, C., Moser, E., & Thurner, S. (2004). Wavelet-based multifractal analysis of fmri time series. *NeuroImage*, 22, 1195–1202. doi:10.1016/j.neuroimage.2004.03.007
- Siegle, G. J., Thompson, W., Carter, C. S., Steinhauer, S. R., & Thase, M. E. (2007). Increased amygdala and decreased dorsolateral prefrontal bold responses in unipolar depression: Related and independent features. *Biological Psychiatry*, 61, 198–209. doi:10.1016/j.biopsych.2006.05.048
- Sokunbi, M. O., Cameron, G. G., Ahearn, T. S., Murray, A. D., & Staff, R. T. (2015). Fuzzy approximate entropy analysis of resting state fMRI signal complexity across the adult life span. *Medical Engineering & Physics*, 37, 1082–1090. doi:10.1016/j.medengphy.2015.09.001
- Sotres-Bayon, F., Bush, D. E. A., & LeDoux, J. E. (2004). Emotional perseveration: An update on prefrontal-amygdala interactions in fear extinction. *Learning & Memory*, 11, 525–535. doi:10.1101/lm.79504
- Stam, C. J. (2005). Nonlinear dynamical analysis of eeg and meg: Review of an emerging field. *Clinical Neurophysiology*, 116, 2266–2301. doi:10.1016/j.clinph.2005.06.011
- Stamkopoulos, T., Diamantaras, K., Maglaveras, N., & Srintzis, M. (1998). Ecg analysis using nonlinear pca neural networks for ischemia detection. *Signal Processing, IEEE Transactions On*, 46, 3058–3067. doi:10.1109/78.726818
- Suckling, J., Wink, A. M., Bernard, F. A., Barnes, A., & Bullmore, E. (2008). Endogenous multifractal brain dynamics are modulated by age, cholinergic blockade and cognitive performance. *Journal of Neuroscience Methods*, 174, 292–300. doi:10.1016/j.jneumeth.2008.06.037
- Thurner, S., Windischberger, C., Moser, E., & Barth, M. (2002). *Fractal noise maps reveal human brain activity*. Technical report.
- Tolkunov, D., Rubin, D., & Lilianne R, M.-P. (2010). Power spectrum scale invariance quantifies limbic dysregulation in trait anxious adults using fmri: Adapting methods optimized for characterizing autonomic dysregulation to neural dynamic time series. *Neuroimage*, 50, 72–80. doi:10.1016/j.neuroimage.2009.12.021
- Tschacher, W., Scheier, C., & Hashimoto, Y. (1997). Dynamical analysis of schizophrenia courses. *Biological Psychiatry*, 41, 428–437. doi:10.1016/S0006-3223(96)00039-X
- Turner, B. M., Paradiso, S., Marvel, C. L., Pierson, R., Boles Ponto, L. L., Hichwa, R. D., & Robinson, R. G. (2007). The cerebellum and emotional experience. *Neuropsychologia*, 45, 1331–1341. doi:10.1016/j.neuropsychologia.2006.09.023
- Volz, K. G., Schubotz, R. I., & Cramon, D. (2005). Variants of uncertainty in decision-making and their neural correlates. *Brain Research Bulletin*, 67, 403–412. doi:10.1016/j.brainresbull.2005.06.011
- Wang, Z., Yin, L., Childress, A. R., & Detre, J. A. (2014). Brain entropy mapping using fMRI. *Plos One*, 9, e89948. doi:10.1371/journal.pone.0089948
- Wink, A.-M., Bullmore, E., Barnes, A., Bernard, F., & Suckling, J. (2008). Monofractal and multifractal dynamics of low frequency endogenous brain oscillations in functional MRI. *Human Brain Mapping*, 29, 791–801. doi:10.1002/hbm.20593
- Xiao-Su, H., Hong, K.-S., & Ge, S. S. (2011). Recognition of stimulus-evoked neuronal optical response by identifying chaos levels of near-infrared spectroscopy time series. *Neuroscience Letters*, 504, 115–120. doi:10.1016/j.neulet.2011.09.011

Appendix A

Time series were preprocessed as described in Section 2, with an additional normalization for standard deviation (see below). For a voxel-wise time series $u = (u_1, \dots, u_N)$, and for a fixed integer “bin size” $m \geq 1$ and a fixed “filter level” $r > 0$, the approximate entropy is defined as follows. For $x_i = (u_i, \dots, u_{i+m-1})$, consider:

$$C_i^{m,r}(u) = \frac{\#\{j \text{ such that } d(x_i, x_j) \leq r\}}{N - m + 1}$$

where $\#$ designates cardinality of a set, and $d(x_i, x_j)$ represents the maximum distance between corresponding components of x_i and x_j . Then, we can define:

$$\Phi^{m,r}(u) = \frac{\sum_{i=1}^{N-m+1} \log C_i^{m,r}(u)}{N - m + 1}$$

Finally, the approximate entropy for the given parameters m and r is

$$\text{ApEn}^{m,r}(u) = \Phi^{m,r}(u) - \Phi^{m+1,r}(u)$$

For infinite time series $u = (u_1, \dots, u_N, \dots)$, this becomes in the limit the theoretical Eckmann–Ruelle entropy:

$$E - R(u) = \lim_{r \rightarrow 0} \lim_{m \rightarrow \infty} \lim_{N \rightarrow \infty} [\Phi^{m,r}(u) - \Phi^{m+1,r}(u)]$$

Intuitively, the E–R entropy and its ApEn computational variation for finite time series measure the (logarithmic) likelihood that patterns which are close will remain close in the future. However, despite similarities in their definitions, $\text{ApEn}^{m,r}$ is not intended as an approximation of the E–R entropy. While a nonzero value for the E–R entropy ensures that a deterministic system is chaotic, ApEn cannot identify chaos. ApEn should be regarded as a family of statistics rather than a unique measure. That is, the actual value of the ApEn for a specific parameter pair (m, r) is largely irrelevant in and of itself; rather, $\text{ApEn}^{m,r}$ is intended for comparisons between signals when using the same (m, r) . It was shown that the optimal value of m (i.e., the value where ApEn is most stable to changes in m) is the maximum m for which $2^{2^m} < N$ (where N is the length of the time series) (Pincus & Singer, 1996). Computations in empirical data suggested that an appropriate range for the noise filter r is 20–40% of the standard deviation of the signal (Pincus, 1991).

In our dataset, we computed ApEn for each voxel, using $m = 2$ and $r = 0.3$, after previously normalizing all our time series to unit standard deviation. The normalization was performed in order to avoid simply capturing differences in the standard deviation of the series when applying r as the same fraction of standard deviation for all signals. As in the case of PSSI, we then thresholded our three-dimensional ApEn brain maps, finely tuning the threshold until separate clusters emerged (Figure A1). Clusters with low ApEn were found in frontal and orbito-

frontal cortices of both subjects. In addition, subject D exhibited additional low ApEn clusters in the hippocampus and in the precuneus, and subject T showed an additional cluster with low ApEn in the cerebellum (Table A1). This is in agreement with existing results, showing the neo-cortex to have lower entropy than the rest of the brain, with some of the lowest regions located in the precuneus and the orbito-frontal cortex (Wang et al., 2014). The differences between subjects point toward an emphasized default (precuneus) and limbic function (hippocampus) in D, versus increased regularity in prefrontal regions in T.

There are known similarities and differences between the dynamic trends that can be best captured using ApEn (which is a phase space measure, incorporating signal amplitudes) and PSSI (which is computed in the frequency domain) (Pincus & Goldberger, 1994). While the clusters found with ApEn are different than those identified using PSSI, the results agree qualitatively, in that they identify more efficient excitatory emotion regulatory regions in stress high responders, and more efficient inhibitory regions in nonresponders.

Appendix B

To obtain our power spectra, we used the fft method of finding the square moduli of the Fourier coefficients. However, there are other power spectrum estimators, which typically use averaging or windowing to eliminate asymptotic bias. In our original 2009 study on PSSI (Tolkunov et al., 2010), we used windowing (the Welch periodogram) when computing the spectra. We switched to the fft estimator in our subsequent paper (Rădulescu et al., 2012), after demonstrating that for our particular data characteristics, the results were comparable between the two methods, and thus the additional noise-averaging obtained by windowing was not necessary in order to detect the PSSI clusters. We have henceforth chosen to consistently use fft in all our analyses on similar datasets. This conveniently eliminates the need for choosing a window size or type, as well as facilitates the comparison of results across different studies. While, in particular, we applied fft in the current analysis, we wish to demonstrate in this section that the results remain qualitatively similar when using instead a Welch periodogram approach.

We computed the PSSI slopes based on a Welch periodogram, using eight windows with 50% overlap. As expected, the slopes using the Welch method were not identical with the values that we obtained using fft. We noticed, however, that an appropriate adjustment of the threshold value from $\tau = -1.75$ to $\tau = -1.5$ accounted for this range shift, and in the end, the clusters identified for each subject were very similar between the two methods. In other words, while windowing did lead to changes in the log–log slopes, the between-voxel differences in these slopes (and ultimately the thresholded results) were comparable. This comparison is illustrated in Figure A2. The clusters detected with the fft method are shown in red, and those detected with the Welch method are shown in green (with significant overlaps), with subject D represented on the left, and subject T on the right.

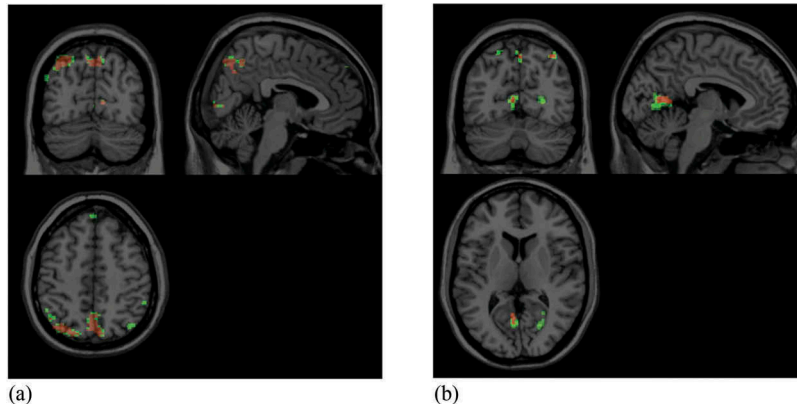


Figure A1. Partial view of the contiguous clusters of volume $V > 3^3$ with $\text{ApEn} < \tau$: for subject D, with threshold $\tau = 1.1$ (left); for subject T, with $\tau = 0.96$ (right). The clusters are described in Table A1.

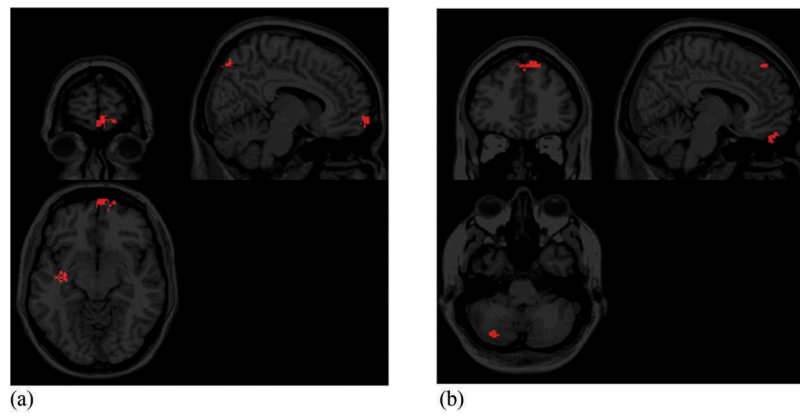


Figure A2. Comparison of clusters obtained with fft versus Welch estimators. The fft clusters, computed with threshold $\tau = -1.75$, are shown in red; the Welch clusters, computed with threshold $\tau = -1.5$, are shown in green. (a) Cluster overlap for subject D; (b) Cluster overlap for subject T.

Table A1. Contiguous clusters larger than $V = 3^3$, whose voxels were identified to have $\text{ApEn} < 1.1$ (for subject D) and $\text{ApEn} < 0.96$ (for subject T).

	Tal coordinates	Anatomical region	Volume (in voxels)
Subject D			
Cluster 1	[30 -14 -11]	Hippocampus L	106
Cluster 2	[-10 74 -5]	Frontal Med/Sup, Mid Orb R	180
Cluster 3	[-8 -69 48]	Precuneus L, R	89
Subject T			
Cluster 1	[30 -70 -35]	Cerebellum Crus L	77
Cluster 2	[-14 56 -16]	Frontal Sup Orb R	109
Cluster 3	[12 74 11]	Frontal Sup L	117
Cluster 4	[-12 39 48]	Frontal Sup/Med R	119